Computationally efficient beam elements for accurate stresses in sandwich laminates and laminated composites with delaminations

R.M.J. Groh[a,*] and A. Tessler[b]

[a]*Advanced Composites Centre for Innovation and Science, University of Bristol, Queen's Building, University Walk, Bristol, BS8 1TR, UK*
[b]*Structural Mechanics and Concepts Branch, NASA Langley Research Center, Mail Stop 190, Hampton, VA 23681-2199, USA*

Abstract

Laminated composites are prone to delamination failure due to the lack of reinforcement through the thickness. Therefore, during the design process the initiation and propagation of delaminations should be accounted for as early as possible. This paper presents computationally efficient nine degree-of-freedom (dof) and eight-dof shear locking-free beam elements using the mixed form of the refined zigzag theory ($\text{RZT}^{(m)}$). The corresponding nine-dof and eight-dof elements use the anisoparametric and constrained anisoparametric interpolation schemes, respectively, to eliminate shear locking in slender beams. The advantage of the present element over previous RZT beam elements is that no post-processing is required to accurately model the transverse shear stress while maintaining the computational efficiency of a low-order beam element. Comparisons with high-fidelity finite element models and three-dimensional elasticity solutions show that the elements can robustly and accurately predict the displacement field, axial stress and transverse shear stress through the thickness of a sandwich beam or a composite laminate with an embedded delamination. In fact, the accuracy and computational efficiency of predicting stresses in laminates with embedded delaminations make the present elements attractive choices for RZT-based delamination initiation and propagation methodologies available in the literature.

Keywords: Shear locking, Zigzag theory, Reissner's mixed variational theorem, Delamination

1. Introduction

Laminated composites are prone to delamination failure due to the lack of reinforcement through the thickness, and this failure mode adversely affects the structural integrity of composite struc-

tures. Hence, the initiation and propagation of delaminations should be accounted for at the early stages in the design process. In this respect, tools for accurate stress predictions are an important prerequisite.

Currently, the standard approach in industry is to use three-dimensional finite element (3-D FE) models or layerwise theories to predict accurate 3-D stress fields. At the preliminary design stage, detailed yet computationally expensive 3-D FE solutions are prohibitive for rapid design as meshes with multiple elements per layer are typically required for converged results. Therefore, 3-D layerwise models are often only used on a component-scale level in areas of high stress concentration or for safety-critical components.

For most composite laminates the thickness dimension is at least an order of magnitude smaller than representative in-plane dimensions, which allows these structures to be modeled as thin beams, plates or shells. This feature facilitates a reduction from a 3-D problem to a 2-D one coincident with a chosen reference axis or surface. The major advantage of this approximation is a significant reduction in the total number of variables and computational effort required.

In multi-layered composite structures the effects of transverse shear and normal deformations are especially pronounced because the ratios of longitudinal to transverse moduli are approximately one order of magnitude greater than for isotropic materials ($E_{xx}^{iso}/G_{xz}^{iso} = 2.6$, $E_{11}/G_{13} \approx 140/5 = 28$ and $E_{xx}^{iso}/E_{zz}^{iso} = 1$, $E_{11}/E_{33} \approx 150/10 = 15$). Second, differences in layerwise transverse shear and normal moduli lead to abrupt changes in the slopes of the three displacement fields u_x, u_y, u_z at layer interfaces. This is known as the zigzag phenomenon (see Figure 1) and, as shown by Demasi [1], the zigzag form of the displacements u_x, u_y and u_z can be derived directly from interfacial continuity requirements of the through-thickness stresses.

The classical theory of plates (CTP) [2, 3] and its extension to laminated structures, namely classical laminate analysis (CLA) [4], are commonly regarded as inadequate for predicting accurate through-thickness stresses under the conditions described in the previous paragraph. This theory neglects the effects of transverse shear and transverse normal strains, the displacement fields neglect the zigzag effect, and the transverse displacement is assumed to be constant through the thickness.

To overcome these deficiencies a large number of approximate higher-order 2-D theories have been formulated with the aim of predicting accurate 3-D stress fields while maintaining low computational expense. Refinements of CLA along these lines have focused mainly on displacement-based

models due to the relatively intuitive physical meaning of the displacement variables that govern the distortion of the plate cross-section. These theories extend from first-order shear deformation theories by Mindlin [5] and Yang, Norris and Stavsky [6] to higher-order Levinson-Reddy-type shear deformation models that enforce vanishing shear strains at the top and bottom surfaces in the displacement field *a priori* [7, 8], and further to generalized higher-order theories that do not make this initial assumption and may account for transverse normal deformation, i.e. thickness stretching [9, 10]. Finally, starting with the works of Lekhnitskii [11] and Ambartsumyan [12] in the Russian literature, and Di Sciuva [13] and Murakami [14] in the Western literature, attempts were made to incorporate changes in the layerwise slopes of the in-plane displacements u_x and u_y via unknown zigzag bending rotations multiplied by layup-dependent zigzag functions. Since then, more accurate zigzag functions have been proposed by Tessler et al. [15–18] and Icardi [19], with the latter work providing the most recent assessment of different zigzag theories.

A fundamental characteristic of purely displacement-based theories is that all strains and stresses are derived from the displacement assumptions using the kinematic and constitutive equations, respectively, and transverse strains and transverse stresses are typically not recovered accurately in this manner [20]. More accurate transverse stresses can be recovered *a posteriori* by integrating the in-plane stresses in Cauchy's 3-D indefinite equilibrium equations [21], and various techniques exist to achieve this within the displacement-based finite element method (FEM) [22–25]. The disadvantage of this technique is that the post-processed transverse stresses no longer satisfy the underlying equilibrium equations, and are therefore variationally inconsistent.

The aforementioned post-processing operation can be precluded if independent assumptions for the transverse stresses are made. This results in a mixed displacement/stress-based approach, whereby the governing equilibrium equations and boundary conditions are derived by means of a mixed-variational statement. For example, in the Hellinger-Reissner mixed variational principle [26, 27], the strain energy is expressed in complementary form in terms of in-plane and transverse stresses, and Cauchy's 3-D equilibrium equations are introduced as constraints via Lagrange multipliers. This has the advantage that the six stress fields are always equilibrated and provide very accurate predictions of through-thickness stresses [28, 29].

Forty years after publishing his work on the Hellinger-Reissner principle, Reissner [30] had the insight that it is sufficient to make separate assumptions for the transverse stresses because

only these have to be specified independently to guarantee interfacial continuity requirements. This variational statement is known as Reissner's mixed-variational theorem (RMVT), and makes model assumptions for the three displacements u_x, u_y, u_z and independent assumptions for the transverse shear stresses τ_{xz}, τ_{yz} and transverse normal stress σ_z. Compatibility of the transverse strains from kinematic relations, i.e. from u_x, u_y and u_z, and constitutive equations, i.e. from τ_{xz}, τ_{yz} and σ_z, is enforced by means of Lagrange multipliers.

Murakami [14] was one of the first authors to use RMVT for composites and simultaneously enhance the axiomatic first-order displacement field of Yang, Norris and Stavsky [6] by including a zigzag function. Murakami made piecewise-parabolic assumptions for the transverse shear stresses that satisfy the interlaminar and surface traction conditions. Even so, Murakami's transverse shear stress assumptions lead to poor results for laminates with more than three layers [31] because the assumptions do not equilibrate with the axial stresses at each point through the thickness, but rather only in an average sense via the equivalent-single layer equilibrium equations. Thus, the particular choice of the transverse shear stress assumption is of great importance when applying RMVT.

Furthermore, Murakami's zigzag function suffers from certain limitations for sandwiches with large face-to-core stiffness ratios and arbitrary layups as it is not based on actual transverse shear moduli that drive the underlying physics of the problem [31, 32]. As an alternative, the zigzag function of the refined zigzag theory (RZT) developed by Tessler, Di Sciuva and Gherlone [15–18] may be used. In this theory, the zigzag slopes $\beta_i^{(k)}$ are defined by the difference between the transverse shear rigidities $G_{iz}^{(k)}$ of layer k, and the effective transverse shear rigidity G_i of the entire layup

$$\beta_i^{(k)} = \frac{G_i}{G_{iz}^{(k)}} - 1, \quad \text{where} \quad G_i = \left[\frac{1}{2h} \sum_{k=1}^{N_l} \frac{2h^{(k)}}{G_{iz}^{(k)}} \right]^{-1}, \quad i = x, y \tag{1}$$

where N_l is the total number of layers, and $2h^{(k)}$ and $2h$ are the thickness of layer k and total laminate thickness, respectively. Thus, the zigzag slopes $\beta_i^{(k)}$ vanish when the transverse shear modulus of a layer is equal to the effective "spring-in-series" stiffness G_i, and a non-zero value quantifies the normalized difference from G_i.

The early displacement-based versions of RZT require stress recovery steps for accurate transverse stress predictions. To remedy this deficiency, Tessler [33] developed a mixed-variational approach of RZT, known as RZT$^{(m)}$ for 1-D beams using RMVT. The novelty of this work is

4

that the assumption for the transverse shear stresses is based on the equilibrium condition between in-plane stress and the transverse shear stress. As a result of enforcing the critical condition of equilibrated stresses, very accurate through-thickness stresses can be computed directly from the underlying model assumptions. In recent work, the formulation was further extended to 2-D plates [34].

A driving factor in the development of RZT and RZT$^{(m)}$ is that the theories be amenable to the development of C^0-continuous finite elements. A nine degree-of-freedom (dof) and eight-dof beam element based on RZT were developed by Gherlone et al. [35] using the anisoparametric interpolation scheme proposed by Tessler and Dong [36] where the transverse displacement variable w is interpolated with one polynomial order greater than the bending rotation θ to prevent shear locking. These lower order two- and three-noded elements were then extended to an entire class of higher-order elements by Di Sciuva et al. [37]. The same interpolation scheme was also used in a version of RZT$^{(m)}$ with cubic in-plane displacement field and quadratic transverse displacement [38].

The aim of this paper is to develop robust beam elements based on Tessler's RZT$^{(m)}$ that provide computationally efficient in-plane stress and transverse shear stress predictions for laminates and sandwich beams with embedded delaminations which can be modeled explicitly within RZT by means of thin resin-rich layers. The motivation for this work is that accurate stress field predictions within these interply resin-rich zones are critical for predicting accurately the onset and propagation of delaminations using the damage frameworks developed for RZT [39, 40].

The rest of the paper is structured as follows. Section 2 provides a background to RZT which is then extended to RZT$^{(m)}$ in Section 3. An eight-dof constrained anisoparametric and nine-dof anisoparametric beam element based on RZT$^{(m)}$ are then developed in Section 4. Detailed comparisons of through-thickness stresses with benchmark 3-D elasticity and 3-D FE results are presented in Section 5 and a discussion of the accuracy of the different interpolation schemes is provided. Finally, conclusions are drawn in Section 6.

2. Refined zigzag theory from the principle of virtual displacements

Following the standard definition of the displacement field in RZT we make the assumption that

$$u_x^{(k)}(x, z) = u(x) + z\theta(x) + \phi^{(k)}(z)\psi(x) \tag{2a}$$

$$u_z(x) = w(x) \tag{2b}$$

where u and w are the axial displacement and average transverse displacement of the reference plane, respectively, θ is the average bending rotation, ψ is the zigzag rotation and $\phi^{(k)}$ is the layerwise zigzag function of RZT. The zigzag function is defined by

$$\phi^{(k)}(z) = (z + h)\left(\frac{G}{G_{xz}^{(k)}} - 1\right) + \sum_{i=2}^{k} 2h^{(i-1)}\left(\frac{G}{G_{xz}^{(i-1)}} - \frac{G}{G_{xz}^{(k)}}\right) \tag{3}$$

where the summation term vanishes for $k = 1$, and G is the equivalent "springs-in-series" transverse shear rigidity of the laminate defined by

$$G = \left[\frac{1}{h}\sum_{k=1}^{N_l}\frac{h^{(k)}}{G_{xz}^{(k)}}\right]^{-1}. \tag{4}$$

Given the piecewise linear form of the zigzag function, Eq. (3) can be written in a more concise form as

$$\phi^{(k)}(z) = z\beta^{(k)} + \alpha^{(k)} \tag{5}$$

where

$$\beta^{(k)} = \frac{\mathrm{d}\phi^{(k)}}{\mathrm{d}z} = \frac{G}{G_{xz}^{(k)}} - 1 \tag{6a}$$

$$\alpha^{(k)} = \beta^{(k)}h + \sum_{i=2}^{k} 2h^{(i-1)}\left(\frac{G}{G_{xz}^{(i-1)}} - \frac{G}{G_{xz}^{(k)}}\right). \tag{6b}$$

Here $\beta^{(k)}$ is the layerwise slope of the zigzag function and $\alpha^{(k)}$ enforces interlaminar continuity.

For a linear elastic material undergoing infinitesimal strains and small displacements, the axial stress is derived from Hooke's law as follows

$$\sigma_{xx}^{(k)} = E^{(k)}\epsilon_{xx}^{(k)} = E^{(k)}\frac{\partial u_x^{(k)}}{\partial x} = E^{(k)}\left(u_{,x} + z\theta_{,x} + \phi^{(k)}(z)\psi_{,x}\right) \tag{7}$$

where the comma notation has been used to denote partial differentiation. For a beam in plane

6

strain in the width direction $E^{(k)} = E_{xx}^{(k)}/\left(1 - \nu_{xy}^{(k)}\nu_{yx}^{(k)}\right)$ and for a beam in plane stress $E^{(k)} = E_{xx}^{(k)}$, where $E_{xx}^{(k)}$ is the Young's modulus of the kth layer in the axial direction, and $\nu_{xy}^{(k)}$ and $\nu_{yx}^{(k)}$ are the major and minor Poisson's ratios, respectively.

Similarly, the transverse shear stress is given by

$$\tau_{xz}^{(k)} = G_{xz}^{(k)}\gamma_{xz}^{(k)} = G_{xz}^{(k)}\left(\frac{\partial u_x^{(k)}}{\partial z} + \frac{\partial u_z}{\partial x}\right) = G_{xz}^{(k)}\left(\gamma + \beta^{(k)}\psi\right) \tag{8}$$

where $G_{xz}^{(k)}$ is the transverse shear modulus of the kth layer in the xz-plane, and

$$\gamma = w_{,x} + \theta \tag{8a}$$

is an average shear strain [33].

In the RZT beam theory a set of stress resultants is defined by integrating the stresses over the cross-sectional area, A, of the beam. Hence,

$$\begin{pmatrix} N & M & M^\phi & V & V^\phi \end{pmatrix}^\top = \int_A \boldsymbol{f}^{(k)\top}\begin{Bmatrix} \sigma_{xx}^{(k)} \\ \tau_{xz}^{(k)} \end{Bmatrix}\mathrm{d}A = \left(b\int_{-h}^{h}\boldsymbol{f}^{(k)\top}\boldsymbol{C}\boldsymbol{f}^{(k)}\mathrm{d}z\right)\boldsymbol{\epsilon} \tag{9}$$

where b is the uniform width of the beam and the through-thickness matrix $\boldsymbol{f}^{(k)}$, constitutive matrix $\boldsymbol{C}$ and strain vector $\boldsymbol{\epsilon}$ are given by

$$\boldsymbol{f}^{(k)} = \begin{bmatrix} 1 & z & \phi^{(k)}(z) & 0 & 0 \\ 0 & 0 & 0 & 1 & \beta^{(k)} \end{bmatrix}, \qquad \boldsymbol{C} = \begin{bmatrix} E^{(k)} & 0 \\ 0 & G_{xz}^{(k)} \end{bmatrix}, \qquad \boldsymbol{\epsilon} = \begin{pmatrix} u_{,x} & \theta_{,x} & \psi_{,x} & \gamma & \psi \end{pmatrix}^\top. \tag{10}$$

The integral $\boldsymbol{S} = b\int_{-h}^{h}\boldsymbol{f}^{(k)\top}\boldsymbol{C}\boldsymbol{f}^{(k)}\mathrm{d}z$ is the reduced stiffness matrix of the RZT beam theory

$$\boldsymbol{S} = \begin{bmatrix} A_{11} & B_{11} & B_{12} & 0 & 0 \\ B_{11} & D_{11} & D_{12} & 0 & 0 \\ B_{12} & D_{12} & D_{13} & 0 & 0 \\ 0 & 0 & 0 & Q_{11} & Q_{12} \\ 0 & 0 & 0 & Q_{12} & Q_{22} \end{bmatrix} \tag{11}$$

where

$$(A_{11}, B_{11}, B_{12}, D_{11}, D_{12}, D_{13}) = b\int_{-h}^{h}\left(1, z, \phi^{(k)}(z), z^2, z\phi^{(k)}(z), \phi^{(k)^2}(z)\right)E^{(k)}\mathrm{d}z \tag{12a}$$

7

$$(Q_{11}, Q_{12}, Q_{22}) = b \int_{-h}^{h} \left(1, \beta^{(k)}, \phi^{(k)2}\right) G_{xz}^{(k)} \mathrm{d}z. \tag{12b}$$

A set of variationally consistent governing field equations and boundary conditions is derived by substituting the RZT stresses and strains into the principle of virtual displacements. Hence,

$$\delta\Pi = \int_V \left[\delta\epsilon_{xx}^{(k)\top}\sigma_{xx}^{(k)} + \delta\gamma_{xz}^{(k)\top}\tau_{xz}^{(k)}\right]\mathrm{d}V - \iint \left[\hat{T}_t \delta u_x^{(N_l)}(x, h) - \hat{T}_b \delta u_x^{(1)}(x, -h) + \left(\hat{P}_t - \hat{P}_b\right)\delta w(x)\right]\mathrm{d}x\mathrm{d}y$$

$$-\int_A \left[-\hat{\sigma}_{xx}^{(k)}(x_a, z)\delta u_x^{(k)}(x_a, z) + \hat{\sigma}_{xx}^{(k)}(x_b, z)\delta u_x^{(k)}(x_b, z) - \hat{\tau}_{xz}^{(k)}(x_a, z)\delta w(x_a) + \hat{\tau}_{xz}^{(k)}(x_b, z)\delta w(x_b)\right]\mathrm{d}A = 0$$

$$\tag{13}$$

where x_a and x_b are the two ends of the beam with $\hat{\sigma}_{xx}^{(k)}(x_a, z)$ and $\hat{\sigma}_{xx}^{(k)}(x_b, z)$ denoting the corresponding prescribed axial stresses, and $\hat{\tau}_{xz}^{(k)}(x_a, z)$ and $\hat{\tau}_{xz}^{(k)}(x_b, z)$ the prescribed transverse shear stresses; $\hat{T}_t$ and $\hat{T}_b$ are the shear tractions along the x-axis at the top and bottom surfaces of the laminate, respectively; and $\hat{P}_t$ and $\hat{P}_b$ are the normal pressures acting on the top and bottom surfaces of the laminate, respectively.

Integrating over the cross-section, performing integration by parts to eliminate derivatives from variations of the functional variables and collecting like terms, we obtain the following set of four equilibrium equations:

$$\delta u: \ N_{,x} + \hat{T}_d = 0, \qquad \delta w: \ V_{,x} + \hat{P} = 0 \tag{14a-b}$$

$$\delta\theta: \ M_{,x} - V + h\hat{T}_s = 0, \qquad \delta\psi: \ M_{,x}^{\phi} - V^{\phi} = 0 \tag{14c-d}$$

where

$$\hat{T}_d = b\left(\hat{T}_t - \hat{T}_b\right), \qquad \hat{T}_s = b\left(\hat{T}_t + \hat{T}_b\right), \qquad \hat{P} = b\left(\hat{P}_t - \hat{P}_b\right). \tag{15}$$

The equilibrium equations in Eq. (14) are used in the next section to derive a more accurate model assumption for the transverse shear stress.

3. Refined zigzag theory based on Reissner's variational principle

The transverse shear stresses in Eq. (8) are layerwise constant functions that do not satisfy the equilibrium of interlaminar and surface tractions. Moreover, these transverse shear stresses vary linearly through the thickness of the beam, whereas from Cauchy's equilibrium equations the linear axial stresses of Eq. (7) are equilibrated by quadratic transverse shear stresses. For these reasons, a

more accurate assumption for the transverse shear stress is needed, and is briefly described herein according to [33].

3.1. Assumed transverse shear stress

Using the insight that the transverse shear stress $\tau_{xz}^{(k)}$ needs to be in equilibrium with the axial stress $\sigma_{xx}^{(k)}$ we use Cauchy's equilibrium equation in Cartesian coordinates

$$\sigma_{xx,x}^{(k)} + \tau_{xz,z}^{(k)} + f_x = 0 \tag{16}$$

to derive a new expression for the transverse shear stresses denoted by $\tau_{xz(e)}^{(k)}$. Disregarding the influence of the body force f_x we have

$$\tau_{xz(e)}^{(k)}(x, z) = -\tau_u^{(k)}(z)u_{,xx}(x) - \tau_\theta^{(k)}(z)\theta_{,xx}(x) - \tau_\psi^{(k)}(z)\psi_{,xx}(x) + f_0(x) \tag{17}$$

where the through thickness functions $\tau_u^{(k)}, \tau_\theta^{(k)}$ and $\tau_\psi^{(k)}$ are defined as

$$\left(\tau_u^{(k)}(z), \tau_\theta^{(k)}(z), \tau_\psi^{(k)}(z)\right) = \left(E_{xx}^{(k)}z + a^{(k)}, \; E_{xx}^{(k)}\frac{z^2}{2} + b^{(k)}, \; E_{xx}^{(k)}\beta^{(k)}\frac{z^2}{2} + E_{xx}^{(k)}\alpha^{(k)}z + c^{(k)}\right) \tag{18}$$

where the terms $a^{(k)}, b^{(k)}$ and $c^{(k)}$ are integration constants that enforce the interlaminar continuity of the shear stress. Hence,

$$\left(a^{(k)}, b^{(k)}\right) = \left(\sum_{i=1}^{k}\left(E_{xx}^{(i-1)} - E_{xx}^{(i)}\right)z_{i-1} + E_{xx}^{(1)}z_0, \; \sum_{i=1}^{k}\left(E_{xx}^{(i-1)} - E_{xx}^{(i)}\right)\frac{z_{i-1}^2}{2} + E_{xx}^{(1)}\frac{z_0^2}{2}\right)$$

$$c^{(k)} = \sum_{i=1}^{k}\left(E_{xx}^{(i-1)}\beta^{(i-1)} - E_{xx}^{(i)}\beta^{(i)}\right)\frac{z_{i-1}^2}{2} + \sum_{i=1}^{k}\left(E_{xx}^{(i-1)}\alpha^{(i-1)} - E_{xx}^{(i)}\alpha^{(i)}\right)z_{i-1} + E_{xx}^{(1)}\beta^{(1)}\frac{z_0^2}{2} + E_{xx}^{(1)}\alpha^{(1)}z_0. \tag{19}$$

Part of the integration constant, namely f_0, has been factored out from $a^{(k)}, b^{(k)}$ and $c^{(k)}$ in order to enforce the condition that the through-thickness integral of the equilibrated transverse shear stress in Eq. (17) is equal to the shear force V:

$$V(x) = \int_{-h}^{h} \tau_{xz(e)}^{(k)}\mathrm{d}A = -b\int_{-h}^{h}\left[\tau_u^{(k)}(z)u_{,xx}(x) + \tau_\theta^{(k)}(z)\theta_{,xx}(x) + \tau_\psi^{(k)}(z)\psi_{,xx}(x)\right]\mathrm{d}z + f_0(x)A. \tag{20}$$

Solving for $f_0(x)$ results in

$$f_0(x) = \frac{V(x)}{A} + \frac{1}{2h}\int_{-h}^{h}\left[\tau_u^{(k)}(z)u_{,xx}(x) + \tau_\theta^{(k)}(z)\theta_{,xx}(x) + \tau_\psi^{(k)}(z)\psi_{,xx}(x)\right]\mathrm{d}z. \tag{21}$$

As a result, we can now enforce equilibrium between the transverse shear force V, bending moment M and the applied surface shear tractions as defined by Eq. (14c). By eliminating V in this manner

$$f_0 = \frac{1}{A}\left(B_{11}u_{,xx} + D_{11}\theta_{,xx} + D_{12}\psi_{,xx} + h\hat{T}_s\right) + \frac{1}{2h}\int_{-h}^{h}\left[\tau_u^{(k)}u_{,xx} + \tau_\theta^{(k)}\theta_{,xx} + \tau_\psi^{(k)}\psi_{,xx}\right]\mathrm{d}z \quad (22)$$

where the bending moment M has been replaced using the constitutive relation Eq. (9). Finally, using the axial equilibrium equation, Eq. (14a), the second derivate of $u_{,xx}$ is eliminated from Eq. (17) and Eq. (22). Using equilibrium equation Eq. (14a) and substituting for N using the constitutive relation Eq. (9), there results

$$u_{,xx} = -\frac{1}{A_{11}}\left(B_{11}\theta_{,xx} + B_{12}\psi_{,xx} + \hat{T}_d\right) \quad (23)$$

which alongside Eq. (17) and Eq. (22) gives

$$\tau_{xz(e)}^{(k)}(x,z) = T_0^{(k)}(x,z) + T_\theta^{(k)}(z)\theta_{,xx}(x) + T_\psi^{(k)}(z)\psi_{,xx}(x) \quad (24)$$

where

$$T_0^{(k)}(x,z) = \frac{\hat{T}_s(x)}{2b} - \frac{\hat{T}_d(x)}{A_{11}}\left[\frac{B_{11}}{A} + \frac{1}{2h}\int_{-h}^{h}\tau_u^{(k)}\mathrm{d}z - \tau_u^{(k)}(z)\right] \quad (25a)$$

$$T_\theta^{(k)}(z) = -\frac{B_{11}}{A_{11}}\left[\frac{B_{11}}{A} + \frac{1}{2h}\int_{-h}^{h}\tau_u^{(k)}\mathrm{d}z - \tau_u^{(k)}(z)\right] + \frac{D_{11}}{A} + \frac{1}{2h}\int_{-h}^{h}\tau_\theta^{(k)}\mathrm{d}z - \tau_\theta^{(k)}(z) \quad (25b)$$

$$T_\psi^{(k)}(z) = -\frac{B_{12}}{A_{11}}\left[\frac{B_{11}}{A} + \frac{1}{2h}\int_{-h}^{h}\tau_u^{(k)}\mathrm{d}z - \tau_u^{(k)}(z)\right] + \frac{D_{12}}{A} + \frac{1}{2h}\int_{-h}^{h}\tau_\psi^{(k)}\mathrm{d}z - \tau_\psi^{(k)}(z). \quad (25c)$$

As is demonstrated in Appendix A, the above substitution for the integration constant $f_0(x)$ is the critical step in guaranteeing that the transverse shear stress at the bottom and top surfaces of the laminate is always equilibrated with the applied shear tractions $\hat{T}_b$ and $\hat{T}_t$, respectively. In essence, the interlaminar continuity of $\tau_u^{(k)}, \tau_\theta^{(k)}$ and $\tau_\psi^{(k)}$, and the axial equilibrium equation enforced in f_0 ensures that $\tau_{xz(e)}^{(k)}$ satisfies all interlaminar and surface traction conditions. In fact, the mathematical consistency of enforcing the interlaminar and surface traction conditions via the integration constants and the axial equilibrium equation was demonstrated in [31, 41, 42] using a different assumption for the transverse shear stress.

Due to the presence of second-order derivatives in Eq. (24), this shear stress assumption is not amenable to the development of C^0-continuous finite elements. Therefore, the second-order derivatives $\theta_{,xx}$ and $\psi_{,xx}$ are replaced by two unknown functions f_θ and f_ψ to produce a new

10

transverse shear stress assumption

$$\tau_{xz(a)}^{(k)}(x,z) = T_0^{(k)}(x,z) + T_\theta^{(k)}(z)f_\theta(x) + T_\psi^{(k)}(z)f_\psi(x) \tag{26}$$

where f_θ and f_ψ are determined via Reissner's mixed variational statement in the next section and the subscript (a) in $\tau_{xz(a)}^{(k)}$ denotes an assumption. Note that Eq. (26) preserves the same interlaminar continuity characteristics as Eq. (24).

3.2. Reissner's mixed variational statement

In Reissner's mixed variational statement an independent assumption is made for some of the stress fields, typically the transverse shear and/or transverse normal stresses, and the compatibility of the transverse shear/normal strains derived from Hooke's law and the kinematic relations are enforced via Lagrange multipliers. As shown by Reissner [30], the Lagrange multipliers are in fact the corresponding transverse shear/normal stresses. Hence, in the present case the variational statement reads

$$\int_V \left(\sigma_{xx}^{(k)} \delta\epsilon_{xx}^{(k)} + \tau_{xz(a)}^{(k)} \delta\gamma_{xz}^{(k)} \right) \mathrm{d}V + \underline{\int_V \delta\tau_{xz(a)}^{(k)} \left(\gamma_{xz}^{(k)} - \gamma_{xz(a)}^{(k)} \right) \mathrm{d}V} - \delta W_e = 0 \tag{27}$$

where W_e is the work done by the external forces acting on the beam and the Lagrange multiplier part has been underlined. By substituting Eq. (26) we can see that the only variational terms in the Lagrange multiplier part of Eq. (27) are δf_θ and δf_ψ. As these terms do not appear in either the internal nor the external work portions of Eq. (27), the Lagrange multiplier term can be considered separately first. Hence,

$$\iint \left(T_\theta^{(k)} \delta f_\theta + T_\psi^{(k)} \delta f_\psi \right) \left(\gamma + \beta^{(k)}\psi - \Gamma_0^{(k)} - \Gamma_\theta^{(k)} f_\theta - \Gamma_\psi^{(k)} f_\psi \right) \mathrm{d}A\mathrm{d}x \tag{28a}$$

where

$$\Gamma_0^{(k)}(x,z) = \frac{T_0^{(k)}(x,z)}{G_{xz}^{(k)}} = \frac{\hat{T}_s(x)}{2bG_{xz}^{(k)}} - \frac{\hat{T}_d(x)}{A_{11}G_{xz}^{(k)}} \left[\frac{B_{11}}{A} + \frac{1}{2h}\int_{-h}^{h} \tau_u^{(k)}\mathrm{d}z - \tau_u^{(k)}(z) \right]$$

$$= L_1^{(k)}(z)\hat{T}_s(x) + L_2^{(k)}(z)\hat{T}_d(x) \tag{28b}$$

$$\left(\Gamma_\theta^{(k)}(z),\ \Gamma_\psi^{(k)}(z) \right) = \left(\frac{T_\theta^{(k)}(z)}{G_{xz}^{(k)}},\ \frac{T_\psi^{(k)}(z)}{G_{xz}^{(k)}} \right). \tag{28c}$$

11

Factoring out the variations δf_θ and δf_ψ, Eq. (28a) is re-written as

$$\int_{x_a}^{x_b} \delta f_\theta \left[\int_A T_\theta^{(k)} \left(\gamma + \beta^{(k)} \psi - \Gamma_\theta^{(k)} f_\theta - \Gamma_\psi^{(k)} f_\psi \right) \mathrm{d}A - \hat{T}_s \int_A L_1^{(k)} T_\theta^{(k)} \mathrm{d}A - \hat{T}_d \int_A L_2^{(k)} T_\theta^{(k)} \mathrm{d}A \right] \mathrm{d}x +$$

$$\int_{x_a}^{x_b} \delta f_\psi \left[\int_A T_\psi^{(k)} \left(\gamma + \beta^{(k)} \psi - \Gamma_\theta^{(k)} f_\theta - \Gamma_\psi^{(k)} f_\psi \right) \mathrm{d}A - \hat{T}_s \int_A L_1^{(k)} T_\psi^{(k)} \mathrm{d}A - \hat{T}_d \int_A L_2^{(k)} T_\psi^{(k)} \mathrm{d}A \right] \mathrm{d}x$$

$$(29)$$

and because the variations $\delta f_\theta(x)$ and $\delta f_\psi(x)$ are arbitrary over the length of the beam we have the following set of coupled algebraic equations

$$\begin{bmatrix} \int T_\theta^{(k)} \Gamma_\theta^{(k)} \mathrm{d}A & \int T_\theta^{(k)} \Gamma_\psi^{(k)} \mathrm{d}A \\ \int T_\psi^{(k)} \Gamma_\theta^{(k)} \mathrm{d}A & \int T_\psi^{(k)} \Gamma_\psi^{(k)} \mathrm{d}A \end{bmatrix} \begin{Bmatrix} f_\theta \\ f_\psi \end{Bmatrix} = \begin{bmatrix} \int T_\theta^{(k)} \mathrm{d}A & \int T_\theta^{(k)} \beta^{(k)} \mathrm{d}A \\ \int T_\psi^{(k)} \mathrm{d}A & \int T_\psi^{(k)} \beta^{(k)} \mathrm{d}A \end{bmatrix} \begin{Bmatrix} \gamma \\ \psi \end{Bmatrix} -$$

$$\hat{T}_s \begin{Bmatrix} \int T_\theta^{(k)} L_1^{(k)} \mathrm{d}A \\ \int T_\psi^{(k)} L_1^{(k)} \mathrm{d}A \end{Bmatrix} - \hat{T}_d \begin{Bmatrix} \int T_\theta^{(k)} L_2^{(k)} \mathrm{d}A \\ \int T_\psi^{(k)} L_2^{(k)} \mathrm{d}A \end{Bmatrix}. \quad (30)$$

Equations (30) are readily solved for f_θ and f_ψ which are then substituted into Eq. (26) to define $\tau_{xz(a)}^{(k)}$ as

$$\tau_{xz(a)}^{(k)}(x,z) = \bar{T}_0^{(k)}(x,z) + \bar{T}_\gamma^{(k)}(z)\gamma(x) + \bar{T}_\psi^{(k)}(z)\psi(x) \quad (31)$$

where $\bar{T}_0^{(k)}, \bar{T}_\gamma^{(k)}$ and $\bar{T}_\psi^{(k)}$ are obtained by solving Eq. (30).

4. Beam finite element formulations

4.1. Stiffness matrix and external force vector

Having obtained an expression for the assumed transverse shear stress $\tau_{xz(a)}^{(k)}$ from the Lagrange multiplier portion of Reissner's mixed variational statement, the internal and external virtual work expressions of Eq. (27) are now used to develop the eight- and nine-dof, shear locking-free beam elements. Using Eq. (27) and substituting the RZT strain expressions from Eq. (7) and Eq. (8)

12

gives

$$\delta W_i = \int_V \delta \begin{bmatrix} \epsilon_{xx}^{(k)} & \gamma_{xz}^{(k)} \end{bmatrix} \begin{Bmatrix} \sigma_{xx}^{(k)} \\ \tau_{xz(a)}^{(k)} \end{Bmatrix} \mathrm{d}V = \int_{x_a}^{x_b} \int_A \delta \begin{Bmatrix} u_{,x} \\ \theta_{,x} \\ \psi_{,x} \\ w_{,x} \\ \theta \\ \psi \end{Bmatrix}^{\top} \begin{bmatrix} 1 & 0 \\ z & 0 \\ \phi^{(k)} & 0 \\ 0 & 1 \\ 0 & 1 \\ 0 & \beta^{(k)} \end{bmatrix} \begin{Bmatrix} \sigma_{xx}^{(k)} \\ \tau_{xz(a)}^{(k)} \end{Bmatrix} \mathrm{d}A\mathrm{d}x = \int_{x_a}^{x_b} \delta\boldsymbol{\omega}^{\top} \boldsymbol{R}\mathrm{d}x$$

(32)

where $\boldsymbol{\omega}$ is a vector of strain components and $\boldsymbol{R}$ is a vector of stress resultants

$$\boldsymbol{\omega} = \begin{bmatrix} u_{,x} & \theta_{,x} & \psi_{,x} & w_{,x} & \theta & \psi \end{bmatrix}^{\top}$$ (33)

$$\boldsymbol{R} = \begin{bmatrix} N & M & M^{\phi} & V & V & V^{\phi} \end{bmatrix}^{\top} = \int_A \begin{bmatrix} \sigma_{xx}^{(k)} & z\sigma_{xx}^{(k)} & \phi^{(k)}\sigma_{xx}^{(k)} & \tau_{xz(a)}^{(k)} & \tau_{xz(a)}^{(k)} & \beta^{(k)}\tau_{xz(a)}^{(k)} \end{bmatrix}^{\top} \mathrm{d}A.$$

(34)

Note that the transverse shear force V is included twice in the resultant vector $\boldsymbol{R}$ of Eq. (34) to allow for a straightforward computational implementation.

As the axial stress remains unchanged from Eq. (7), the definitions of the membrane force N and bending moments M and M^{ϕ} remain unchanged. Hence, the axial reduced stiffness terms of Eq. (11) also remain the same. However, the transverse shear reduced stiffness terms change due to the new definition of $\tau_{xz(a)}^{(k)}$

$$(Q_{10}^m, Q_{11}^m, Q_{12}^m) = b \int_{-h}^{h} \left(\bar{T}_0^{(k)}, \bar{T}_\gamma^{(k)}, \bar{T}_\psi^{(k)} \right) \mathrm{d}z$$ (35)

$$(Q_{20}^m, Q_{21}^m, Q_{22}^m) = b \int_{-h}^{h} \beta^{(k)} \left(\bar{T}_0^{(k)}, \bar{T}_\gamma^{(k)}, \bar{T}_\psi^{(k)} \right) \mathrm{d}z.$$ (36)

Therefore the stress resultants $\boldsymbol{R}$ are related to the strain components $\boldsymbol{\omega}$ as follows,

$$\boldsymbol{R} = \begin{Bmatrix} N \\ M \\ M^{\phi} \\ V \\ V \\ V^{\phi} \end{Bmatrix} = \begin{bmatrix} A_{11} & B_{11} & B_{12} & 0 & 0 & 0 \\ B_{11} & D_{11} & D_{12} & 0 & 0 & 0 \\ B_{12} & D_{12} & D_{13} & 0 & 0 & 0 \\ 0 & 0 & 0 & Q_{11}^m & Q_{11}^m & Q_{12}^m \\ 0 & 0 & 0 & Q_{11}^m & Q_{11}^m & Q_{12}^m \\ 0 & 0 & 0 & Q_{21}^m & Q_{21}^m & Q_{22}^m \end{bmatrix} \boldsymbol{\omega} + \begin{Bmatrix} 0 \\ 0 \\ 0 \\ Q_{10}^m \\ Q_{10}^m \\ Q_{20}^m \end{Bmatrix} = \boldsymbol{D}\boldsymbol{\omega} + \boldsymbol{D}_0.$$

(37)

13

Using Eq. (37) the internal virtual work expression given by Eq. (32) is simplified to

$$\delta W_i = \int_{x_a}^{x_b} \left(\delta \boldsymbol{\omega}^\top \boldsymbol{D} \boldsymbol{\omega} + \delta \boldsymbol{\omega}^\top \boldsymbol{D}_0 \right) \mathrm{d}x. \tag{38}$$

In a displacement-based finite element setting the displacement field in each element is interpolated using element shape functions and nodal variables. Therefore, the element displacements $\boldsymbol{u}^{(e)} = (u,\ w,\ \theta,\ \psi)^{(e)}$ and strain components $\boldsymbol{\omega}^{(e)} = (u_{,x},\ \theta_{,x},\ \psi_{,x},\ w_{,x},\ \theta,\ \psi)^{(e)}$ can be expressed as

$$\boldsymbol{u}^{(e)} = \boldsymbol{H}^{(e)} \bar{\boldsymbol{u}}^{(e)}, \qquad \boldsymbol{\omega}^{(e)} = \boldsymbol{B}^{(e)} \bar{\boldsymbol{u}}^{(e)} \tag{39}$$

where $\bar{\boldsymbol{u}}^{(e)}$ are the nodal variables, and $\boldsymbol{H}^{(e)}$ and $\boldsymbol{B}^{(e)}$ are the displacement and strain shape function matrices of element e, respectively, which are defined for the eight- and nine-dof beam elements described in the next two sections. Substituting Eq. (39) into the internal virtual work expression given by Eq. (38), results in

$$\delta W_i = \delta \bar{\boldsymbol{u}}^{(e)\top} \left(\int_{x_a}^{x_b} \boldsymbol{B}^{(e)\top} \boldsymbol{D}^{(e)} \boldsymbol{B}^{(e)} \mathrm{d}x \right) \bar{\boldsymbol{u}}^{(e)} + \delta \bar{\boldsymbol{u}}^{(e)\top} \int_{x_a}^{x_b} \boldsymbol{B}^{(e)\top} \boldsymbol{D}_0^{(e)} \mathrm{d}x \tag{40}$$

and because $\delta \bar{\boldsymbol{u}}^{(e)}$ is arbitrary we have

$$\boldsymbol{f}_{int}^{(e)} = \boldsymbol{K}_L^{(e)} \boldsymbol{u}^{(e)} \quad \text{with} \quad \boldsymbol{K}_L^{(e)} = \int_{x_a}^{x_b} \boldsymbol{B}^{(e)\top} \boldsymbol{D}^{(e)} \boldsymbol{B}^{(e)} \mathrm{d}x, \tag{41}$$

$$\boldsymbol{f}_\tau^{(e)} = \int_{x_a}^{x_b} \boldsymbol{B}^{(e)\top} \boldsymbol{D}_0^{(e)} \mathrm{d}x \tag{42}$$

where $\boldsymbol{K}_L^{(e)}$ is the linear stiffness matrix and $\boldsymbol{f}_\tau^{(e)}$ is an external force vector due to applied surface shear tractions. Finally, the virtual work done by the external forces is derived from Eq. (13) as

$$\delta W_e = - \int \left[\hat{T}_d \delta u + \frac{h}{2} \hat{T}_s \delta \theta + \hat{P} \delta w \right] \mathrm{d}x + \hat{N}(x_a)\delta u(x_a) - \hat{N}(x_b)\delta u(x_b) + \hat{M}(x_a)\delta\theta(x_a) - \hat{M}(x_b)\delta\theta(x_b)$$
$$+ \hat{M}^\phi(x_a)\delta\psi(x_a) - \hat{M}^\phi(x_b)\delta\psi(x_b) + \hat{V}(x_a)\delta w(x_a) - \hat{V}(x_b)\delta w(x_b). \tag{43}$$

Note that the distributed loads in the integral of Eq. (43) do not feature the term $\delta\psi$ since the zigzag function $\phi^{(k)}$, by definition, vanishes on the top and bottom surfaces of the laminate. Introducing

14

the element discretization into the external virtual work expression of Eq. (43) we have

$$\delta W_e = -\int_{x_a}^{x_b} \delta \begin{bmatrix} u & \theta & w \end{bmatrix} \begin{Bmatrix} \hat{T}_d \\ h\hat{T}_s \\ \hat{P} \end{Bmatrix} \mathrm{d}x + \delta \begin{bmatrix} u & \theta & w & \psi \end{bmatrix}_{x_a} \begin{Bmatrix} \hat{N} \\ \hat{M} \\ \hat{M}^\phi \\ \hat{V} \end{Bmatrix}_{x_a} - \delta \begin{bmatrix} u & \theta & w & \psi \end{bmatrix}_{x_b} \begin{Bmatrix} \hat{N} \\ \hat{M} \\ \hat{M}^\phi \\ \hat{V} \end{Bmatrix}_{x_b}$$

$$= -\delta \bar{\boldsymbol{u}}^{(e)\top} \int_{x_a}^{x_b} \hat{\boldsymbol{H}}^{(e)\top} \hat{\boldsymbol{q}}^{(e)} \mathrm{d}x + \delta \bar{\boldsymbol{u}}^{(e)\top} \left[\boldsymbol{H}^{(e)}(x_a)^\top \hat{\boldsymbol{Q}}_a^{(e)} - \boldsymbol{H}^{(e)}(x_b)^\top \hat{\boldsymbol{Q}}_b^{(e)} \right] \tag{44}$$

where $\hat{\boldsymbol{H}}^{(e)}$ is the shape function matrix $\boldsymbol{H}^{(e)}$ that only includes the rows corresponding to u, w and θ. Also vector $\hat{\boldsymbol{q}}^{(e)}$ includes the applied surface tractions, whereas vectors $\hat{\boldsymbol{Q}}_a$ and $\hat{\boldsymbol{Q}}_b$ feature the applied nodal forces. Finally, the external force vector is identified from Eq. (44) as

$$\boldsymbol{f}_{ext}^{(e)} = \int_{x_a}^{x_b} \hat{\boldsymbol{H}}^{(e)\top} \hat{\boldsymbol{q}}^{(e)} \mathrm{d}x - \boldsymbol{H}^{(e)}(x_a)^\top \boldsymbol{Q}_a^{(e)} + \boldsymbol{H}^{(e)}(x_b)^\top \boldsymbol{Q}_b^{(e)}. \tag{45}$$

Thus, by combining Eq. (41), Eq. (42) and Eq. (45), and assembling the contributions from all elements we arrive at the usual linear algebraic problem of the finite element method

$$\boldsymbol{K}_L \bar{\boldsymbol{u}} = \boldsymbol{f}_{ext} - \boldsymbol{f}_\tau. \tag{46}$$

4.2. Element interpolation

Most Timoshenko-type beam elements using the typical linear or quadratic Lagrange shape functions and full Gaussian integration produce overly stiff results (with near-zero bending curvature) as the thickness to length ratio approaches zero. This type of behavior is known as shear locking and, as pointed out by Tessler and Dong [36], occurs because the shear strain $\gamma = w_{,x} + \theta$ is interpolated using two inconsistent polynomials. Namely, if w and θ are interpolated using the same linear or quadratic shape functions then the order of the polynomial approximating $w_{,x}$ will be one order lower than the polynomial approximating θ, and hence the pure bending state of $w_{,x} \to -\theta$ cannot be represented. If the polynomial order of w and θ is large, say of the fifth order, this condition can be met with negligible error, but for lower order linear and quadratic elements this is not the case.

In an anisoparametric interpolation strategy, w is interpolated using a polynomial one degree greater than the polynomial interpolating θ, and therefore one more degree of freedom is required for w than any of the other variables. As a result, the transverse shear strain γ and the transverse

shear force V are interpolated with a polynomial one order greater than the axial strain and bending moment. To obtain an element with a standard nodal configuration, it is possible to *constrain* the element by coupling the interpolation of w to the rotation θ, and in the case of RZT also to the zigzag rotation ψ. This coupling is achieved by reducing the polynomial degree of the shear strain or shear force, and thereby removing the extra w degree of freedom.

4.2.1. Three-node, nine-dof anisoparametric element

In the anisoparametric setting the lowest order element is a two-node beam with an extra node for the w degree of freedom. Hence, (u, w, θ, ψ) are defined at the two end nodes and w is also defined at a central node. In this case the nodal dof vector, $\bar{\boldsymbol{u}}^{(e)}$, element shape function matrix $\boldsymbol{H}^{(e)}$ and strain matrix $\boldsymbol{B}^{(e)}$ are defined as

$$\bar{\boldsymbol{u}}^{(e)} = \begin{bmatrix} u_1 & w_1 & \theta_1 & \psi_1 & w_3 & u_2 & w_2 & \theta_2 & \psi_2 \end{bmatrix}^\top \tag{47}$$

$$\boldsymbol{H}^{(e)} = \begin{bmatrix} H_1^L & 0 & 0 & 0 & 0 & H_2^L & 0 & 0 & 0 \\ 0 & H_1^Q & 0 & 0 & H_3^Q & 0 & H_2^Q & 0 & 0 \\ 0 & 0 & H_1^L & 0 & 0 & 0 & 0 & H_2^L & 0 \\ 0 & 0 & 0 & H_1^L & 0 & 0 & 0 & 0 & H_2^L \end{bmatrix} \tag{48}$$

$$\boldsymbol{B}^{(e)} = \frac{2}{L^{(e)}} \begin{bmatrix} H_{1,\xi}^L & 0 & 0 & 0 & 0 & H_{2,\xi}^L & 0 & 0 & 0 \\ 0 & 0 & H_{1,\xi}^L & 0 & 0 & 0 & 0 & H_{2,\xi}^L & 0 \\ 0 & 0 & 0 & H_{1,\xi}^L & 0 & 0 & 0 & 0 & H_{2,\xi}^L \\ 0 & H_{1,\xi}^Q & 0 & 0 & H_{3,\xi}^Q & 0 & H_{2,\xi}^Q & 0 & 0 \\ 0 & 0 & \dfrac{L^{(e)}}{2}H_1^L & 0 & 0 & 0 & 0 & \dfrac{L^{(e)}}{2}H_2^L & 0 \\ 0 & 0 & 0 & \dfrac{L^{(e)}}{2}H_1^L & 0 & 0 & 0 & 0 & \dfrac{L^{(e)}}{2}H_2^L \end{bmatrix} \tag{49}$$

where $L^{(e)}$ is the length of an element, the superscripts L and Q refer to the standard linear and quadratic Lagrange shape functions, respectively, defined in terms of the natural coordinate $\xi \in [-1, 1]$ and the subscripts refer to the corresponding node numbers with the comma notation denoting differentiation:

$$\left\{ H_1^L,\ H_2^L \right\} = \left\{ \frac{1}{2}\left(1 - \xi\right),\ \frac{1}{2}\left(1 + \xi\right) \right\} \tag{50a}$$

$$\left\{ H_1^Q,\ H_2^Q,\ H_3^Q \right\} = \left\{ \frac{1}{2}\xi\left(\xi - 1\right),\ 1 - \xi^2,\ \frac{1}{2}\xi\left(\xi + 1\right) \right\}. \tag{50b}$$

Also note that in all the integrals in Eq. (41), (42) and (45) the differential $\mathrm{d}x$ is replaced with the transformation to natural coordinates $L^{(e)}/2\mathrm{d}\xi$ and the limits of integration change from $[x_a, x_b]$ to $[-1, 1]$. By simple inspection of Eqs. (33), (37) and (38) with the shape functions above, we can see that the resultants N, M and M^ϕ are constant over the beam domain ($u_{,x}$, $\theta_{,x}$ and $\psi_{,x}$ are constant) but V and V^ϕ are linear ($w_{,x}$, θ and ψ are linear), such that a two-point Gauss integration scheme is required.

4.2.2. Two-node, eight-dof constrained anisoparametric element

In the constrained anisoparametric element the nodal interpolation is recast by either constraining the transverse shear force V, the average shear strain $\gamma = w_{,x} + \theta$ or the zigzag strain measure $\eta = \gamma - \psi$ to be constant across an element. Gherlone et al. [35] have shown that constraining the average shear strain γ to be constant leads to inaccurate results as the zigzag rotation ψ is not included in the constraining equation. Hence, only the constraints V is constant and η is constant are considered herein (see Appendix B for details on the constraining process).

As a result of the constraint equation the deflection dof at the element midspan, w_3, can be condensed out by expressing it in terms of the end-node values of w, θ and ψ. Hence,

$$w_3 = \frac{w_1 + w_2}{2} + \frac{L^{(e)}}{8}\left[\theta_2 - \theta_1 + c\left(\psi_2 - \psi_1\right)\right] \tag{51}$$

where $c = Q_{12}^m/Q_{11}^m = r$ if V is constant and $c = -1$ if η is constant. Therefore, the constrained interpolation for $w(x)$ in terms of the natural coordinate ξ can be expressed as

$$w = H_1^L(\xi)w_1 + H_2^L(\xi)w_2 + \frac{L^{(e)}}{8}H_3^Q\left[\theta_2 - \theta_1 + c\left(\psi_2 - \psi_1\right)\right]. \tag{52}$$

Consequently, the nodal dof vector, $\bar{\boldsymbol{u}}^{(e)}$, element shape function matrix $\boldsymbol{H}^{(e)}$ and strain matrix $\boldsymbol{B}^{(e)}$ are

$$\bar{\boldsymbol{u}}^{(e)} = \begin{bmatrix} u_1 & w_1 & \theta_1 & \psi_1 & u_2 & w_2 & \theta_2 & \psi_2 \end{bmatrix}^\top \tag{53}$$

$$\boldsymbol{H}^{(e)} = \begin{bmatrix} H_1^L & 0 & 0 & 0 & H_2^L & 0 & 0 & 0 \\ 0 & H_1^L & -\dfrac{L^{(e)}}{8}H_3^Q & -c\dfrac{L^{(e)}}{8}H_3^Q & 0 & H_2^L & \dfrac{L^{(e)}}{8}H_3^Q & c\dfrac{L^{(e)}}{8}H_3^Q \\ 0 & 0 & H_1^L & 0 & 0 & 0 & H_2^L & 0 \\ 0 & 0 & 0 & H_1^L & 0 & 0 & 0 & H_2^L \end{bmatrix} \tag{54}$$

$$\boldsymbol{B}^{(e)} = \frac{2}{L^{(e)}} \begin{bmatrix} H_{1,\xi}^L & 0 & 0 & 0 & H_{2,\xi}^L & 0 & 0 & 0 \\ 0 & 0 & H_{1,\xi}^L & 0 & 0 & 0 & H_{2,\xi}^L & 0 \\ 0 & 0 & 0 & H_{1,\xi}^L & 0 & 0 & 0 & H_{2,\xi}^L \\ 0 & H_{1,\xi}^L & -\dfrac{L^{(e)}}{8}H_{3,\xi}^Q & -c\dfrac{L^{(e)}}{8}H_{3,\xi}^Q & 0 & H_{2,\xi}^L & \dfrac{L^{(e)}}{8}H_{3,\xi}^Q & c\dfrac{L^{(e)}}{8}H_{3,\xi}^Q \\ 0 & 0 & \dfrac{L^{(e)}}{2}H_1^L & 0 & 0 & 0 & \dfrac{L^{(e)}}{2}H_2^L & 0 \\ 0 & 0 & 0 & \dfrac{L^{(e)}}{2}H_1^L & 0 & 0 & 0 & \dfrac{L^{(e)}}{2}H_2^L \end{bmatrix}. \quad (55)$$

Again by simple inspection of Eqs. (33), (37) and (41) with the chosen shape functions above, we can show that a two-point Gauss integration scheme is required when $c = r$ and when $c = -1$. As for the nine-dof element, the resultants N, M and M^ϕ for both eight-dof elements are constant over the beam domain because $u_{,x}$, $\theta_{,x}$ and $\psi_{,x}$ are constant. For $c = r$, V is of course constrained to be constant but V^ϕ nevertheless remains linear because $Q_{22}^m - \dfrac{Q_{12}^m Q_{21}^m}{Q_{11}^m} \neq 0$. Hence, constraining V to be constant via the shape functions does not equally constrain V^ϕ because the stiffness terms involved are different. For $c = -1$, both V and V^ϕ are linear over the beam domain. Thus, for both eight-dof elements the stiffness matrix integrand is a quadratic polynomial and a two-point Gauss rule is required to compute this term exactly.

5. Results

The accuracy and robustness of the two eight-dof beam elements, i.e. for $c = r$ (V constant, denoted by $\mathrm{RZT}_{2V}^{(m)}$) and $c = -1$ (η constant, denoted by $\mathrm{RZT}_{2\eta}^{(m)}$) in Eq. (52), and the nine-dof beam element (denoted by $\mathrm{RZT}_3^{(m)}$) are examined by means of a number of benchmark tests. Section 5.1 shows the convergence of the tip deflection and midspan axial stress of a cantilevered beam with increasing mesh density.

In Section 5.2 through-thickness distributions of the axial displacement, axial stress and transverse shear stress of a beam clamped at both ends and loaded by normal pressure and shear tractions on both surfaces is compared against a high-fidelity finite element solution. Finally, in Section 5.3 the beam element results are validated against a closed-form 3-D elasticity solution. These results not only showcase the excellent predictive capabilities of the present beam elements in terms of stresses and displacements, but also demonstrate that the RZT zigzag function can successfully account for the presence of a delamination at very low computational cost.

18

5.1. A convergence study and discussion of interpolation

A convergence study is conducted for a cantilevered beam of length $L = 0.2$ m, depth $2h = 0.04$ m and width $b = 0.04$ m loaded by a tip shear force of $F = 2000$ N in the state of plane stress. The beam comprises three different materials as defined in Table 1 and these form the stacking sequence defined in Table 2 with layers numbered from bottom to top. All stresses, forces and moments are evaluated at the Gauss integration points, where these quantities have optimal accuracy.

Table 1: Mechanical properties of materials a, b and c.

Material	$E_{xx}^{(k)}$ (GPa)	$G_{xz}^{(k)}$ (GPa)
a	73.0	29.2
b	21.9	8.76
c	0.073	0.029

Table 2: Beam stacking sequence for a cantilevered beam starting from the bottom layer.

Layer thicknesses (m)	Materials
[0.004/0.032/0.004]	[a/c/b]

Figure 2a and Figure 2b show, respectively, the convergence of the deflection at the tip of the cantilever and the midspan axial stress at the bottom of the laminate ($z = -h$) with increasing mesh density. The eight-dof beam elements $\text{RZT}_{2V}^{(m)}$ and $\text{RZT}_{2\eta}^{(m)}$ converge at basically the same rate and slightly faster than the nine-dof element $\text{RZT}_3^{(m)}$. The same relative convergence behavior between unconstrained nine-dof and constrained eight-dof classic RZT elements has also been observed in ref. [37].

In Figure 3a the normalized transverse shear force, V/F, is plotted versus the normalized axial coordinate, x/L, of the cantilevered beam. For this problem V is constant along the length of the beam. Both elements provide the correct value of V along the span. To compute V at the clamped end, $x = 0$, Gauss point values can be extrapolated to that location.

Figure 3b depicts the transverse shear stress through the thickness of the cantilevered beam at $x = L/8$. The results for $\text{RZT}_{2V}^{(m)}$ and $\text{RZT}_{2\eta}^{(m)}$ are indistinguishable from each other and correlate closely with a reference solution. The reference solution is obtained using the commercial FE code Abaqus, where a planar slice in the thickness-length plane of the beam was modeled using 326,400 linear reduced integration S4R elements — 1600 elements were used along the length with [21,

19

162, 21] elements through the thickness of the three layers, respectively. All degrees of freedom were constrained at the clamped end and the shear force at the free end was applied as a line load through the thickness.

In the validation examples of Sections 5.2 and 5.3 only the eight-dof beam element $\text{RZT}_{2V}^{(m)}$ and the nine-dof beam element $\text{RZT}_{3}^{(m)}$ are examined. Based on the convergence study presented above, a mesh of 100 elements is used for $\text{RZT}_{2V}^{(m)}$ and a mesh of 74 elements for $\text{RZT}_{3}^{(m)}$. With these meshes the results produced by the two elements are graphically indistinguishable, and hence a single dataset denoted by $\text{RZT}_{(all)}^{m}$ is shown for all results.

In terms of computational efficiency, the high-fidelity Abaqus model is composed of a numerical system with 656,410 dofs (2 dofs per 328,205 nodes) which required around 2 min to solve on a Dell Precision Tower 3620 x64-based PC with an Intel 4-Core i7-6700 CPU at 3.4 GHz with 16.0 GB RAM. The $\text{RZT}_{2V}^{(m)}$ and $\text{RZT}_{3}^{(m)}$ elements feature 404 dofs (4 dofs per 101 nodes) and 374 dofs (4 dofs per 75 end nodes, and 1 dof per 74 central nodes), respectively, and require around 2 seconds of run time in Matlab.

5.2. Clamped-clamped beam with sinusoidal pressure and shear tractions

The second validation example is carried out for a beam of length $L = 1$ m, width $b = 1$ m and thickness $2h = 0.1$ m clamped at both ends, and in a state of plane stress. The beam is loaded by a normal pressure of $\hat{P}_t = -0.5\sin(\pi x)$ MPa and a shear traction of $\hat{T}_t = -4\cos(\pi x)$ MPa on the top surface, a normal pressure of $\hat{P}_b = 0.5\sin(\pi x)$ MPa and a shear traction of $\hat{T}_b = 2\cos(\pi x)$ MPa on the bottom surface.

Results are presented for two different stacking sequences, laminates A and B, shown in Table 3 using the material properties in Table 1. Laminate A is the soft-core non-symmetric stacking sequence used in the previous section and tests the capability of the beam elements to predict displacements and stresses in thick sandwich beams. Laminate B represents a non-symmetric four-layer laminate with an additional thin layer in between the repeating block of a/b layers. As the constitutive properties of this thin layer are orders of magnitude less than the two adjacent a/b-blocks, this layer models a damaged resin-rich zone in between the two blocks and can thus effectively be regarded as a delamination. Hence, laminate B is a test case to demonstrate that the RZT zigzag function can account for changes in the displacement and stress fields due to the presence of a delamination.

20

Table 3: Stacking sequences for the clamped-clamped beam starting from the bottom layer.

Laminate	Layer thicknesses (m)	Materials
A	[0.01/0.08/0.01]	[a/c/b]
B	[0.025/0.025/0.001/0.025/0.025]	[a/b/c/a/b]

The results presented in the figures have been normalized as follows

$$\bar{u}(z) = \frac{10^6 (2h)^2}{|p_0| L^3} u_x^{(k)}(0.25L, z), \quad \bar{\sigma}(z) = \frac{(2h)^2}{|p_0| L^2} \sigma_{xx}^{(k)}(0.5L, z), \quad \bar{\tau}(z) = \frac{1}{|p_0|} \tau_{xz}^{(k)}(0.25L, z), \quad \zeta = \frac{z}{h}$$

$$(56)$$

where p_0 is the magnitude of the total normal pressure, 1 MPa.

The $\text{RZT}_{2V}^{(m)}$ and $\text{RZT}_3^{(m)}$ results are compared against a high-fidelity reference solution obtained using the commercial FE code Abaqus. In this case, a planar slice in the thickness-length plane of the beam was modeled using 326,400 linear reduced integration S4R elements. For both laminate A and B, 1600 elements were used along the length with [21, 162, 21] elements for the layers of laminate A and [50, 50, 4, 50, 50] elements for layers of laminate B. All degrees of freedom were constrained at either end to model the clamped boundary condition, and the tractions on the top and bottom surfaces of the laminate were imposed via line loads.

Figures 4 and 5 compare the through-thickness axial displacement, axial stress and transverse shear stress of the $\text{RZT}^{(m)}$ models against the FE benchmark. In all cases the results closely compare to the reference solutions. What is especially noteworthy is that the piecewise parabolic transverse shear stresses in Figures 4c and 5c are predicted very accurately from the underlying $\text{RZT}^{(m)}$ assumptions without the need for stress-recovery steps. As the transverse shear stress assumption used in the present implementation of RMVT is inherently equilibrated in a local and average sense through the thickness of the laminate, the surface tractions are mathematically guaranteed to be recovered accurately, and as shown in Figures 4c and 5c, this is indeed the case. Table 4 shows that at specific points through the cross-section of the beam the percent differences for the displacement, axial stress and transverse shear stress results are no more than 5% compared to the FE benchmark and are often within 1%.

The presence of the thin and compliant resin layer in laminate B causes a pronounced zigzag function, as shown in Figure 6, which allows the two a/b-blocks in laminate B to slide over each other. In 3-D finite elements the displacement jump across a cohesive layer is often used to predict

21

Table 4: Comparison of normalized displacement, axial stress and transverse shear stress results of $\mathrm{RZT}^{(m)}_{(all)}$ and a 3-D FE reference solution. z_1 is the interface between the bottommost and second plies in the laminates. The axial locations of the quantities $\bar{u}$, $\bar{\sigma}$ and $\bar{\tau}$ are defined explicitly in Eq. (56) as $x = 0.25L$, $0.5L$ and $0.25L$, respectively.

	Laminate A			Laminate B		
	$\mathrm{RZT}^{(m)}_{(all)}$	Reference	Difference (%)	$\mathrm{RZT}^{(m)}_{(all)}$	Reference	Difference (%)
$\bar{u}$ $(z=h)$	2.763×10^{-6}	2.756×10^{-6}	-0.3	5.867×10^{-7}	5.623×10^{-7}	-4.3
$\bar{\sigma}$ $(z=h)$	-0.2608	-0.2615	0.3	-0.06872	-0.06489	-5.9
$\bar{\tau}$ $(z=z_1)$	-2.323	-2.316	-0.3	-2.023	-2.025	0.1

the propagation of delamination damage via a cohesive damage law. In the framework of RZT, a thin resin layer within the stacking sequence can therefore serve the same purpose and the RZT beam elements presented here could be used to predict damage progression in a computationally efficient manner. For example, a continuum damage law can be chosen to govern the degradation process of the resin-rich layer [39]. This displacement jump across the thin resin layer of laminate B is clearly appreciable in Figure 5a.

Figure 5a shows two different displacement distributions. The first using the standard definition of the RZT zigzag function of Eq. (3). The second uses the modified RZT zigzag function defined by Gherlone [32]. The modification by Gherlone is inspired by the phenomenological observation that for laminates with more than three layers an external layer, i.e. $k = 1$ and $k = N_l$, with transverse shear modulus less than the adjacent internal layer, i.e. $k = 2$ and $k = N_l - 1$, will not give rise to a significant zigzag effect. The layers are aptly called externally weak layers (EWLs) and the following modification is made when calculating the RZT zigzag function

- If $N_l > 3$ and $G_{xz}^{(1)} < G_{xz}^{(2)}$, then $G_{xz}^{(1)} = G_{xz}^{(2)}$

- If $N_l > 3$ and $G_{xz}^{(N_l)} < G_{xz}^{(N_l-1)}$, then $G_{xz}^{(N_l)} = G_{xz}^{(N_l-1)}$.

This modification only applies when calculating the zigzag function $\phi^{(k)}$ and the slopes $\beta^{(k)}$ and not any of the actual constitutive matrices. The difference in zigzag functions is evident in Figure 6, where the EWL curve does not show a change of slope at the uppermost interface (the top layer is an EWL), whereas the standard definition of the RZT zigzag function does. For most laminates studied in the literature, e.g. [31–33], Gherlone's modification has lead to superior results for laminates with EWLs. However, Figure 5a shows that when a thin delamination is present, the

original RZT zigzag function leads to slightly more accurate results.

5.3. Simply supported beam with sinusoidal pressure

The final example considers a beam of length $L = 1$ inch, width $b = 0.1$ inch and thickness $2h = 0.1$ inch simply-supported at both ends. The beam is loaded by a sinusoidally varying pressure on the top and bottom surfaces equal to $\hat{P}_t = -1.5 \times 10^6 \sin(\pi x)$ psi and $\hat{P}_b = 1.5 \times 10^6 \sin(\pi x)$ psi, respectively.

For some specific material properties and stacking sequences this problem can be solved using the 3-D elasticity solution by Pagano [43]. Hence, material p_1 in Table 5 corresponds to the high modulus graphite/epoxy composite defined by Pagano [43], material p_2 is a version of p_1 degraded by a factor of 1000 and p_3 represents a low modulus graphite/epoxy composite. Individual layers of these materials comprise the laminates listed in Table 6. Laminate C is the soft-core non-symmetric stacking sequence used in the previous sections, whereas laminate D is a non-symmetric laminate split into two sublaminates by a thin delamination between the first and third layers from the bottom.

Table 5: Mechanical properties of materials p_1, p_2 and p_3.

Material	$E_{xx}^{(k)}$ (psi)	$G_{xz}^{(k)}$ (psi)
p_1	25×10^6	2×10^5
p_2	25×10^3	2×10^2
p_3	8.333×10^6	6.667×10^4

Table 6: Beam stacking sequences for a simply supported beam with applied sinusoidal pressure starting from the bottom layer.

Laminate	Layer thicknesses (in)	Materials
C	[0.01/0.08/0.01]	$[p_1/p_2/p_3]$
D	[0.05/0.001/0.025/0.025]	$[p_1/p_2/p_3/p_1]$

The displacement and stress results are non-dimensionalized using the following expressions

$$\bar{u}(z) = \frac{10^6 (2h)^2}{|p_0| L^3} u_x^{(k)}(0, z), \quad \bar{\sigma}(z) = \frac{(2h)^2}{|p_0| L^2} \sigma_{xx}^{(k)}(0.5L, z), \quad \bar{\tau}(z) = \frac{1}{|p_0|} \tau_{xz}^{(k)}(0, z), \quad \zeta = \frac{z}{h}. \quad (57)$$

Figures 7-8 again show the good correlation of through-thickness displacements, axial stresses and transverse shear stresses of the present beam elements and the benchmark solution. The

displacement jump across the delamination is predicted with high accuracy as shown in Figure 8a. Furthermore, the fully reversed axial stress distributions of the sublaminates in Figure 8b and the two parabolas apexed at the mid-thickness of the sublaminates suggest that the sublaminates are bending independently. Hence, the physical behavior of two sublaminates shearing over each other due to a delamination is modeled correctly.

For this particular problem, the displacement results in Figures 7a and 8a show greater discrepancies as a result of the cubic deformation in the soft core. This effect is known as "stress channeling" [44] and occurs as the orthotropy ratio $\lambda = \dfrac{E_{xx}}{G_{xz}} \left(\dfrac{2h}{L} \right)^2$ increases. The effect can be readily modelled by including a third-order term z^3 in the assumed displacement field of Eq. (2) as demonstrated within RZT by Groh and Weaver [31] and Iurlaro et al. [38]. This effect, however, is not the predominant factor for most composite laminates used in practical industrial applications. Since the aim of this work is a computationally efficient beam element for the purpose of studying delaminations within the framework of RZT, this higher-order effect has been neglected in favor of the reduced computational expense.

6. Conclusions

Laminated composites are prone to delamination failure due to the lack of reinforcement through the thickness, and hence the initiation and propagation of delaminations should be accounted for as early as possible in the design process. In this paper computationally efficient eight degree-of-freedom (dof) and nine-dof elements, that are free of shear locking, were developed based on the mixed form of the refined zigzag theory, $RZT^{(m)}$.

As shown in this study the beam elements can robustly and accurately predict the displacement field, axial stress and transverse shear stress through the thickness of a sandwich beam or a laminate with an embedded delamination. The advantage of the present element over previous beam elements is that no post-processing is required to compute the transverse shear stress accurately while maintaining the computational efficiency of an eight-dof beam or three-noded nine-dof elements. Eliminating the commonly used stress-recovery steps by means of Cauchy's equilibrium equations not only helps to minimize the computational expense but also ensures that the transverse shear stress results are variationally consistent. Indeed, as shown in this paper, using inherently equilibrated shear stress assumptions enabled by Reissner's mixed variational theorem means the surface and interlaminar tractions are mathematically guaranteed to be recovered correctly.

Accurate predictions of stresses within interply resin-rich zones is crucial for accurately predicting the onset and subsequent propagation of delaminations within damage frameworks developed for RZT [39, 40]. Research is currently ongoing to integrate these or other continuum damage models within the present beam elements to model the delamination initiation and propagation of a number of benchmark problems. Future work will also focus on extending the developed damage onset and propagation framework to 2-D plates.
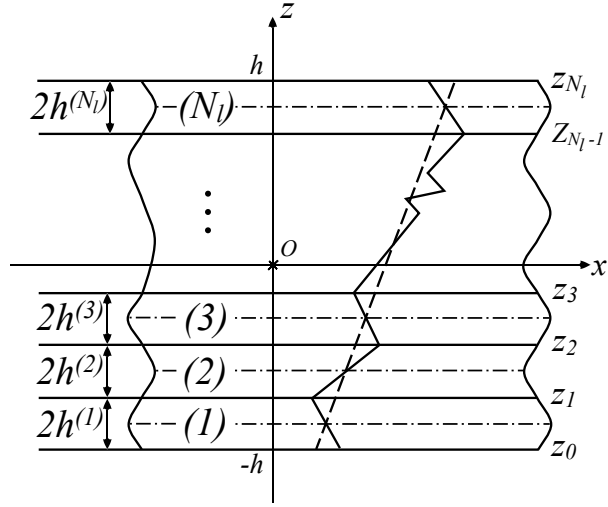
Figure 1: Arbitrary laminate configuration with co-ordinate system and approximate in-plane displacements. The dashed line shows a classical solution of the in-plane displacements, whereas the solid line accounts for zigzag effects.
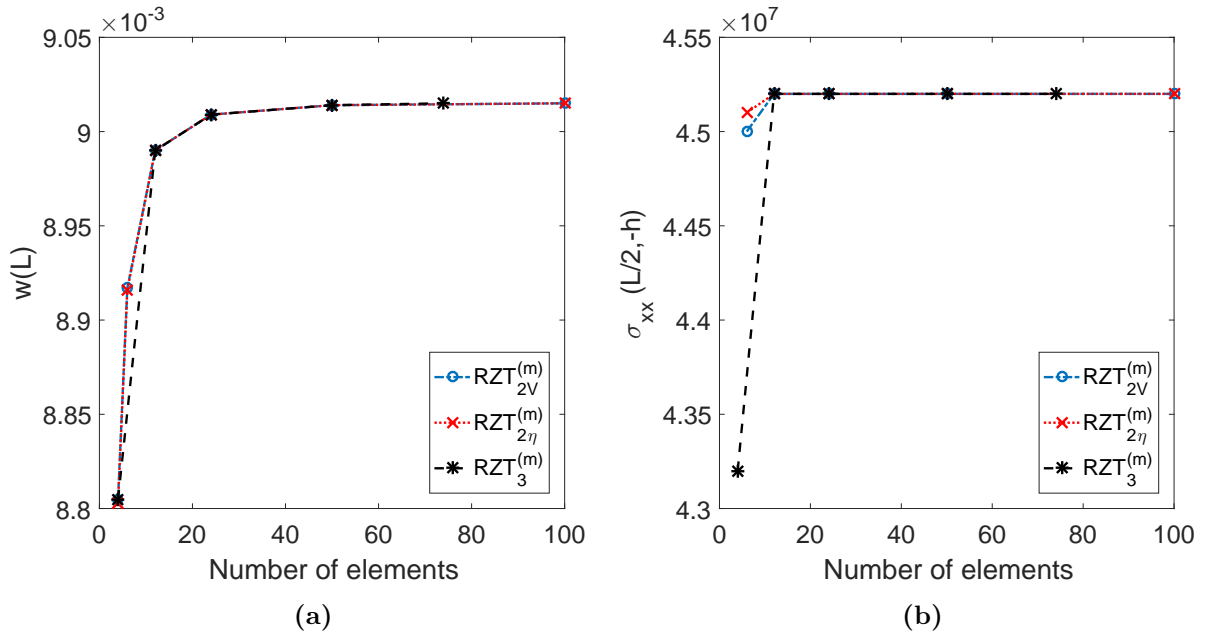
Figure 2: A convergence study of (a) the tip deflection, $w(L)$, and (b) bottom surface axial stress at the midspan, $\sigma_{xx}(L/2, -h)$.
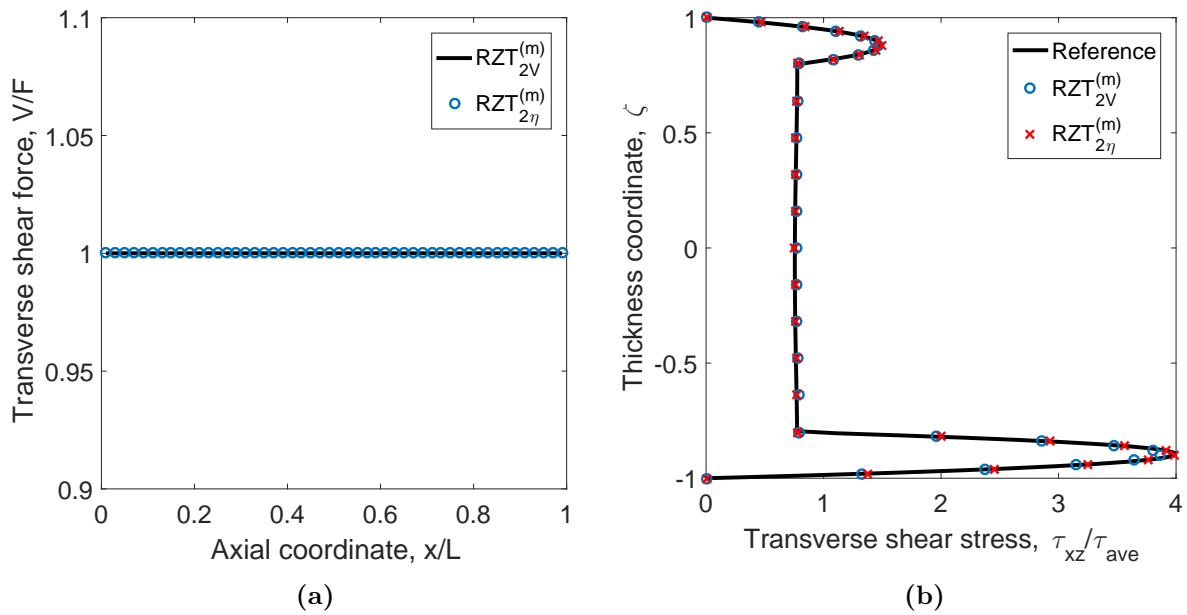
Figure 3: (a) Transverse shear force, V/F, along the length of a cantilevered beam for $\text{RZT}_{2V}^{(m)}$ and $\text{RZT}_{2\eta}^{(m)}$ eight-dof beam elements, and (b) through-thickness distribution of transverse shear stress $\tau_{xz}^{(k)}(L/8, \zeta)/\tau_{ave}$ normalized by the average shear stress $\tau_{ave} = F/(2bh)$.

27

(a)

(b)

(c)
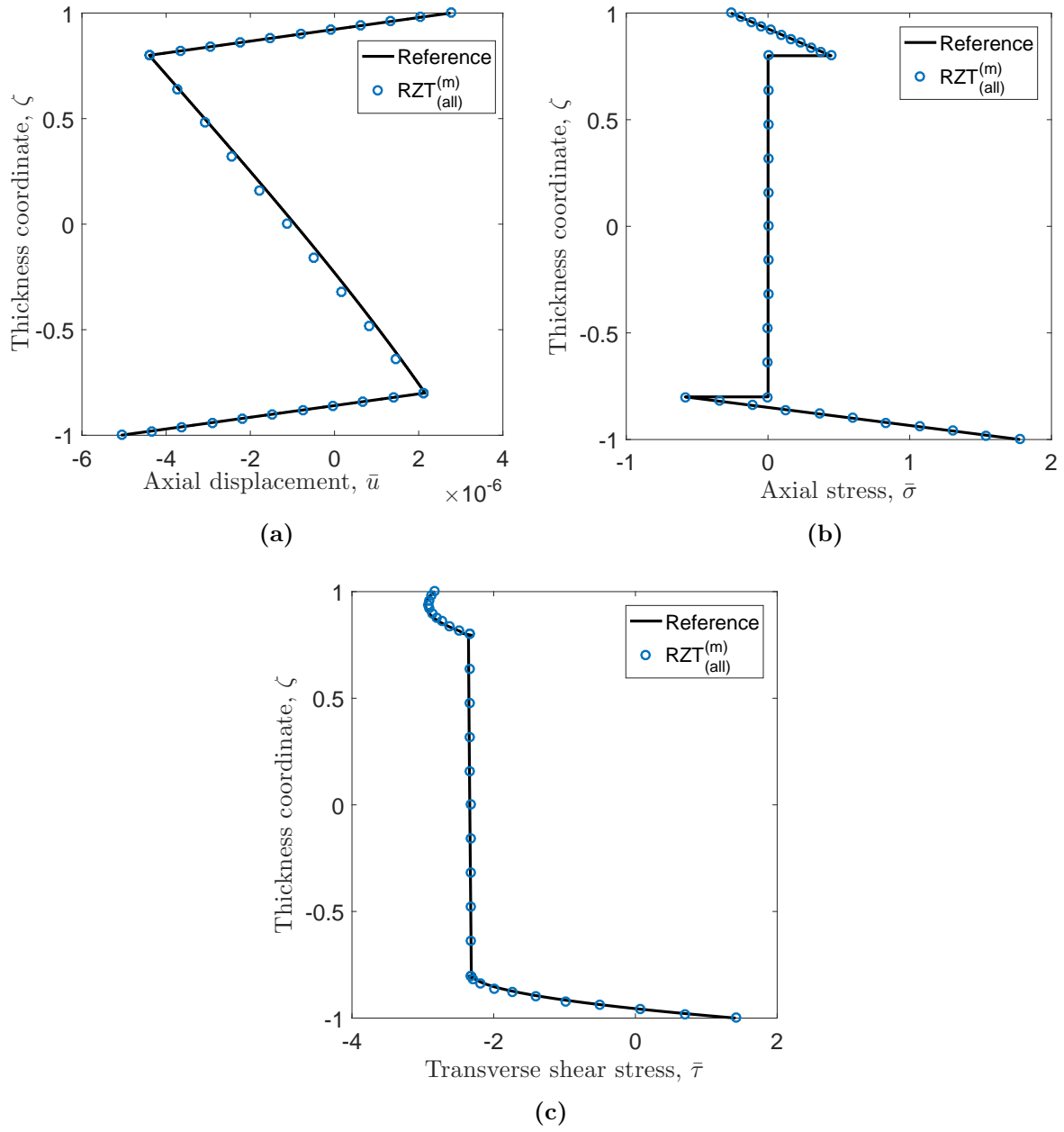
Figure 4: Through-thickness distributions of the normalized (a) axial displacement, $\bar{u}$ $(x = 0.25L)$, (b) axial stress, $\bar{\sigma}$ $(x = 0.5L)$, and (c) transverse shear stress, $\bar{\tau}$ $(x = 0.25L)$, for laminate A.
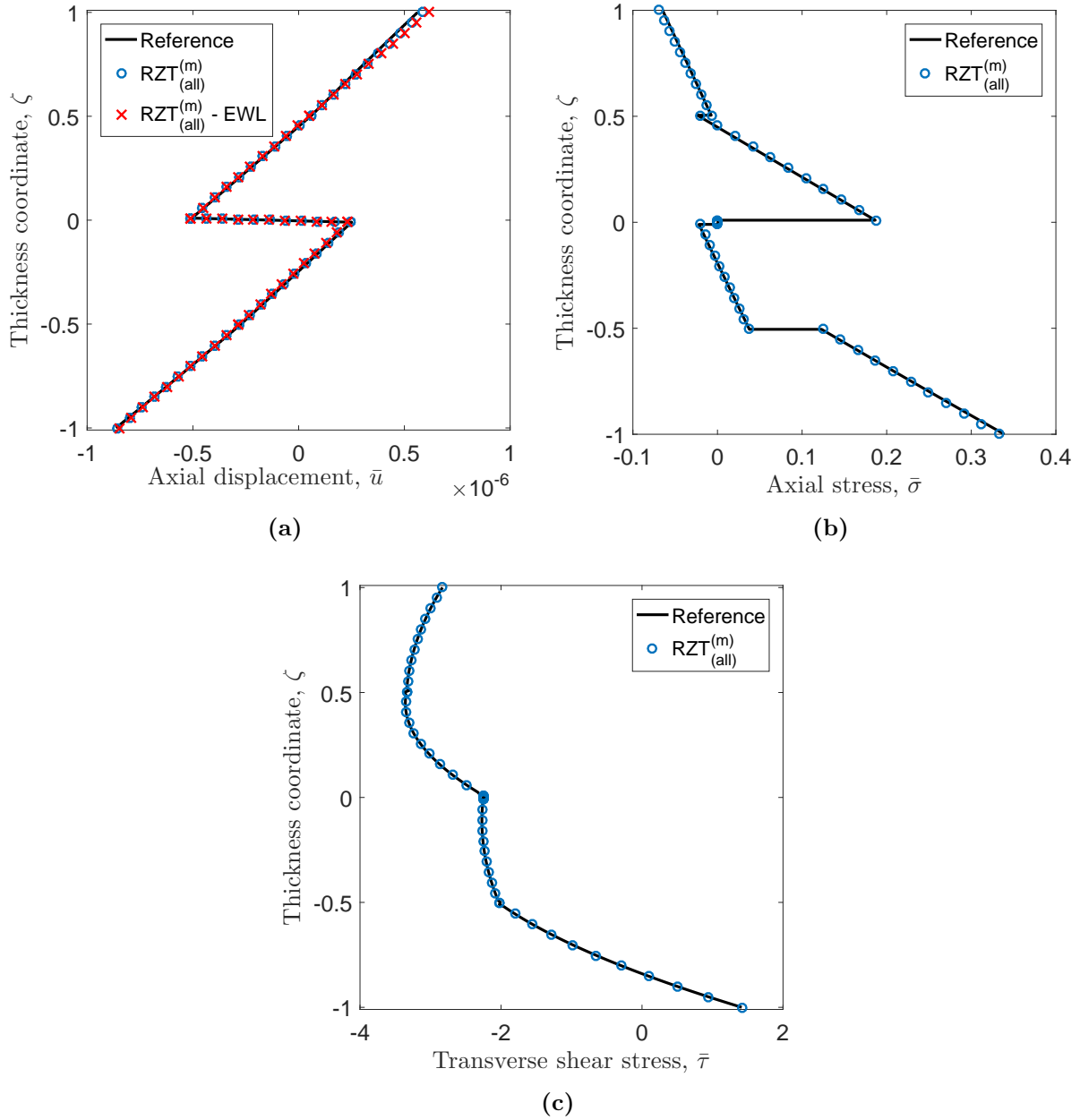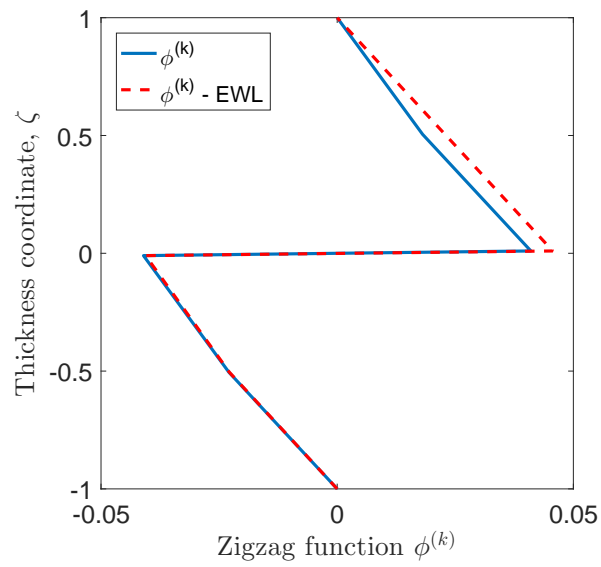
Figure 5: Through-thickness distributions of the normalized (a) axial displacement, $\bar{u}$ $(x = 0.25L)$, (b) axial stress, $\bar{\sigma}$ $(x = 0.5L)$, and (c) transverse shear stress, $\bar{\tau}$ $(x = 0.25L)$, for laminate B.

Figure 6: Laminate B: Through-thickness distributions of the classical RZT zigzag function and the modified zigzag function by Gherlone [32] which accounts for externally weak layers (EWL).
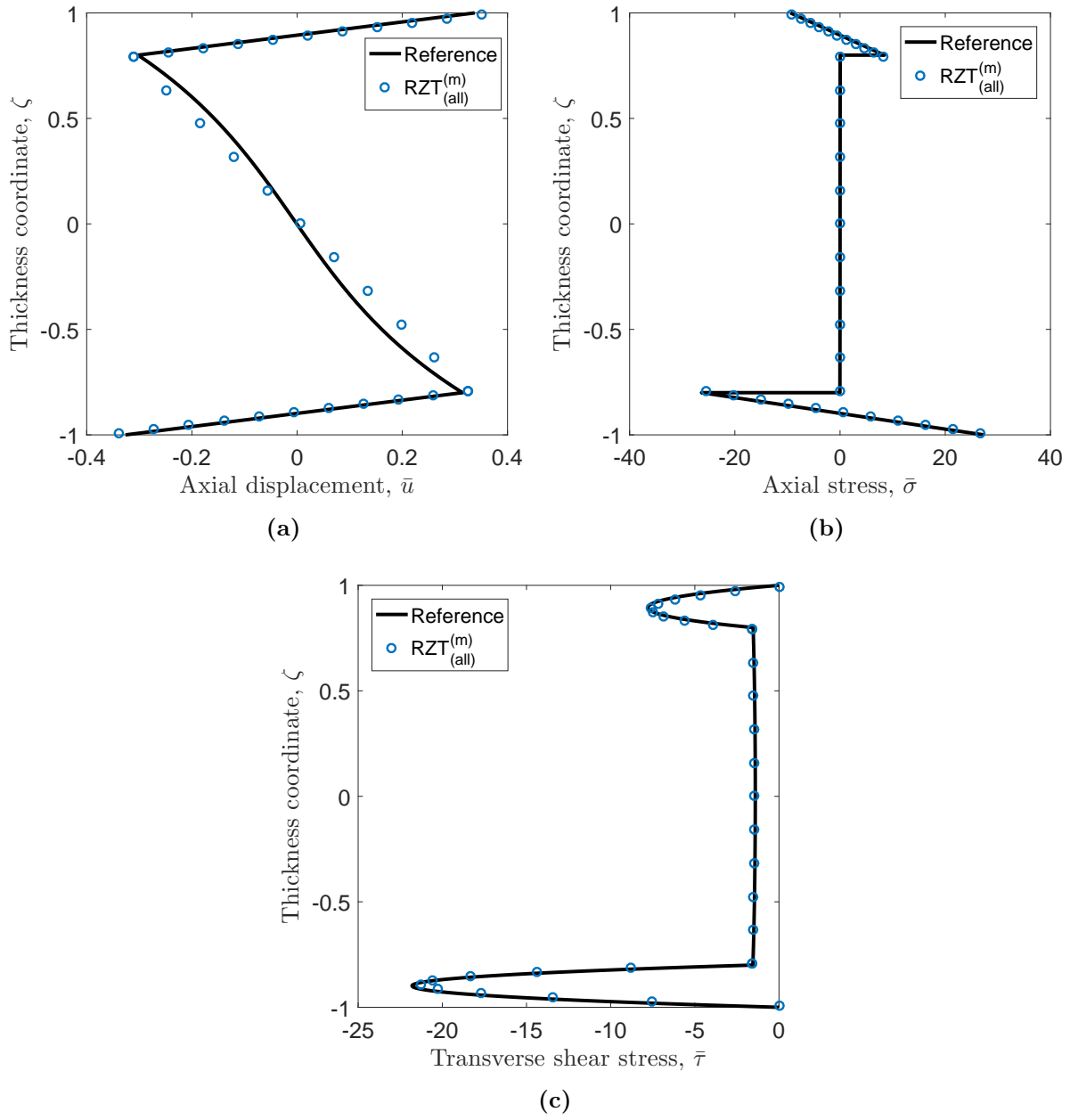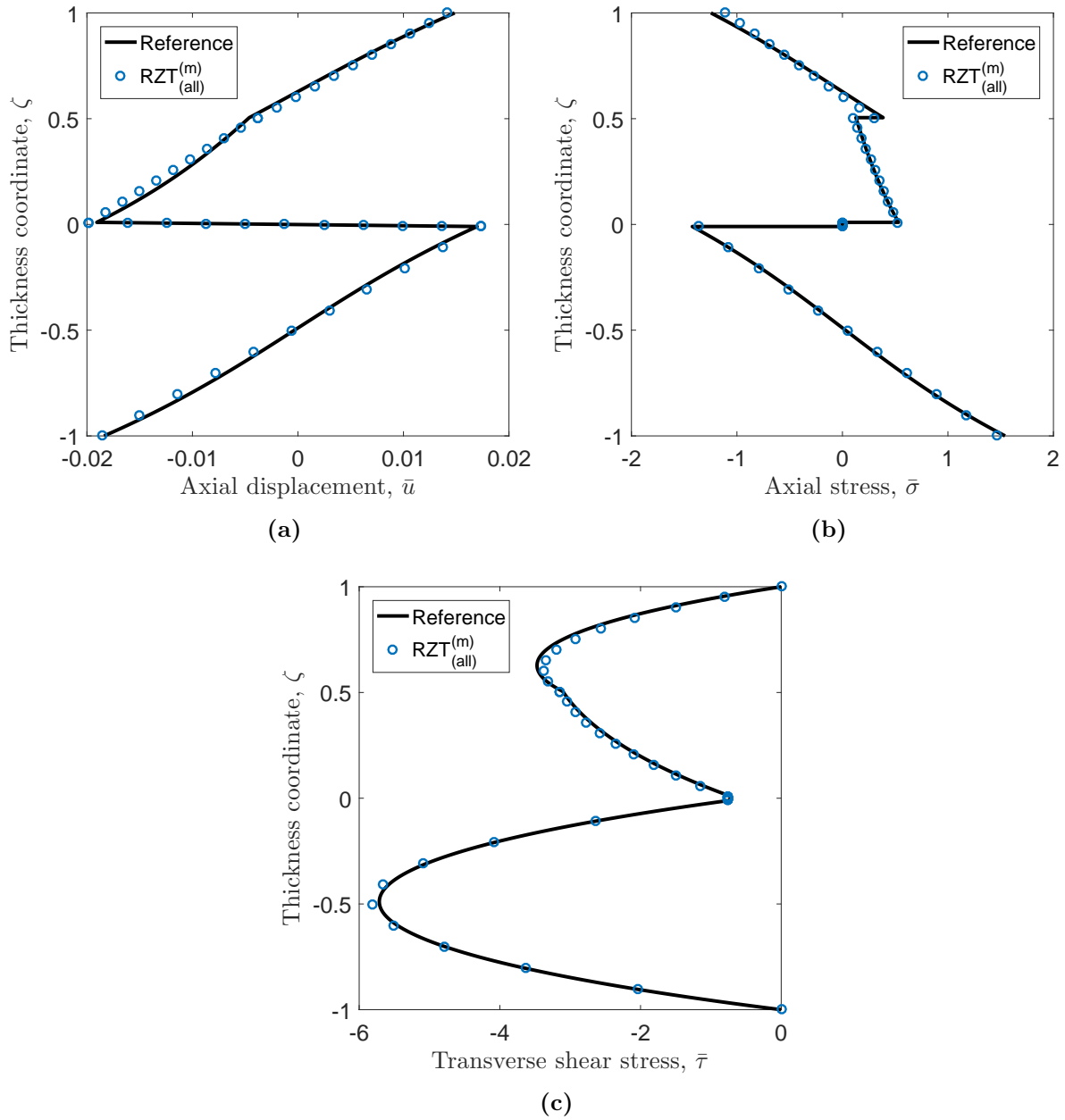
Figure 7: Through-thickness distributions of the normalized (a) axial displacement, $\bar{u}$ $(x = 0)$, (b) axial stress, $\bar{\sigma}$ $(x = 0.5L)$, and (c) transverse shear stress, $\bar{\tau}$ $(x = 0)$, for laminate C.

Figure 8: Through-thickness distributions of the normalized (a) axial displacement, $\bar{u}$ ($x = 0$), (b) axial stress, $\bar{\sigma}$ ($x = 0.5L$), and (c) transverse shear stress, $\bar{\tau}$ ($x = 0$), for laminate D.

Appendix A. Equilibrium of surface tractions

The assumed transverse shear stress is given by Eq. (26)

$$\tau_{xz(a)}^{(k)} = T_0^{(k)} + T_\theta^{(k)} f_\theta + T_\psi^{(k)} f_\psi \tag{A.1}$$

where $T_0^{(k)}$, $T_\theta^{(k)}$ and $T_\psi^{(k)}$ are defined in Eq. (25), respectively.

Interlaminar continuity of Eq. (A.1) is guaranteed by means of the integration constants $a^{(k)}, b^{(k)}$ and $c^{(k)}$ in the expressions for $\tau_u^{(k)}, \tau_\theta^{(k)}$ and $\tau_\psi^{(k)}$, respectively. As shown in the proof below, the equilibrium of the surface tractions is automatically enforced by means of eliminating the integration constant f_0 introduced in Eq. (17). This is achieved by enforcing the through-thickness integral of Eq. (A.1) to equal the RZT transverse shear force V.

To prove that equilibrium of the surface tractions is guaranteed by the assumed transverse shear stress we evaluate Eq. (A.1) at the top and bottom of the laminate. Hence,

$$
\begin{aligned}
\tau_u^{(N_l)}(z_{N_l}) =& E_{xx}^{(N_l)} z_{N_l} + a^{(N_l)} \\
=& E_{xx}^{(N_l)} z_{N_l} + \left(E_{xx}^{(1)} - E_{xx}^{(2)}\right) z_1 + \cdots + \left(E_{xx}^{(N_l-1)} - E_{xx}^{(N_l)}\right) z_{N_l-1} \\
=& E_{xx}^{(1)}(z_1 - z_0) + \cdots + E_{xx}^{(N_l)}(z_{N_l} - z_{N_l-1}) + E_{xx}^{(1)} z_0 \\
=& \frac{A_{11}}{b} + E_{xx}^{(1)} z_0 \tag{A.2}
\end{aligned}
$$

$$\tau_u^{(1)}(z_0) = E_{xx}^{(1)} z_0 + a^{(1)} = E_{xx}^{(1)} z_0. \tag{A.3}$$

Using the same algebraic sequence of steps for $\tau_\theta^{(N_l)}(z_{N_l})$ and $\tau_\theta^{(1)}(z_0)$ we obtain

$$\tau_\theta^{(N_l)}(z_{N_l}) = \frac{B_{11}}{b} + E_{xx}^{(1)} \frac{z_0^2}{2} \tag{A.4}$$

$$\tau_\theta^{(1)}(z_0) = E_{xx}^{(1)} \frac{z_0^2}{2}. \tag{A.5}$$

Similarly, the expressions for $\tau_\psi^{(N_l)}(z_{N_l})$ and $\tau_\psi^{(1)}(z_0)$ result in

$$\tau_\psi^{(N_l)}(z_{N_l}) = \frac{B_{12}}{b} + E_{xx}^{(1)} \left(\beta^{(1)} \frac{z_0^2}{2} + \alpha^{(1)} z_0\right) \tag{A.6}$$

$$\tau_\psi^{(1)}(z_0) = E_{xx}^{(1)} \left(\beta^{(1)} \frac{z_0^2}{2} + \alpha^{(1)} z_0\right). \tag{A.7}$$

Next, we need to express each of the constants

$$\frac{B_{11}}{A} + \frac{1}{2h}\int_{z_0}^{z_{N_l}} \tau_u^{(k)}\mathrm{d}z, \qquad \frac{D_{11}}{A} + \frac{1}{2h}\int_{z_0}^{z_{N_l}} \tau_\theta^{(k)}\mathrm{d}z, \qquad \frac{D_{12}}{A} + \frac{1}{2h}\int_{z_0}^{z_{N_l}} \tau_\psi^{(k)}\mathrm{d}z \qquad (\mathrm{A.8})$$

in terms of components of the higher-order stiffness matrix D, i.e. Eq. (37), and known laminate constants. For the first term in Eq. (A.8) we have

$$\frac{B_{11}}{A} + \frac{1}{2h}\int_{z_0}^{z_{N_l}} \left(E_{xx}^{(k)}z + a^{(k)}\right)\mathrm{d}z = \frac{1}{2bh}\sum_{k=1}^{N_l} bE_{xx}^{(k)}\frac{z_k^2 - z_{k-1}^2}{2} + \frac{1}{2h}\sum_{k=1}^{N_l}\left(E_{xx}^{(k)}\frac{z_k^2 - z_{k-1}^2}{2} + a^{(k)}2h^{(k)}\right)$$

$$= \frac{2}{2h}\sum_{k=1}^{N_l} E_{xx}^{(k)}\frac{z_k^2 - z_{k-1}^2}{2} + \frac{1}{2h}\sum_{k=1}^{N_l} 2h^{(k)}\sum_{i=1}^{k}\left(E_{xx}^{(i-1)} - E_{xx}^{(i)}\right)z_{i-1} + E_{xx}^{(1)}z_0$$

$$= \frac{1}{2h}\left[E_{xx}^{(1)}\left(z_1 + z_0\right)2h^{(1)} + \left\{E_{xx}^{(2)}\left(z_2 + z_1\right) + \left(E_{xx}^{(1)} - E_{xx}^{(2)}\right)z_1\right\}2h^{(2)}+\right.$$

$$\left.\left\{E_{xx}^{(3)}\left(z_3 + z_2\right) + \left(E_{xx}^{(2)} - E_{xx}^{(3)}\right)z_2 + \left(E_{xx}^{(1)} - E_{xx}^{(2)}\right)z_1\right\}2h^{(3)} + \dots\right]$$

$$= \frac{1}{2h}\left[E_{xx}^{(1)}z_1 2h^{(1)} + \left\{E_{xx}^{(2)}z_2 + E_{xx}^{(1)}\left(z_1 - z_0\right)\right\}2h^{(2)} + \left\{E_{xx}^{(3)}z_3 + E_{xx}^{(2)}\left(z_2 - z_1\right) + E_{xx}^{(1)}\left(z_1 - z_0\right)\right\}2h^{(3)} + \dots\right] +$$

$$\frac{1}{2h}E_{xx}^{(1)}z_0\sum_{k=1}^{N_l} 2h^{(k)}$$

$$= \frac{1}{2h}\left[E_{xx}^{(1)}z_1 2h^{(1)} + \left(E_{xx}^{(2)}z_2 + E_{xx}^{(1)}2h^{(1)}\right)2h^{(2)} + \left(E_{xx}^{(3)}z_3 + E_{xx}^{(2)}2h^{(2)} + E_{xx}^{(1)}2h^{(1)}\right)2h^{(3)} + \dots\right] + E_{xx}^{(1)}z_0$$

$$= \frac{1}{2h}\left[E_{xx}^{(1)}2h^{(1)}\left(z_1 + \sum_{k=2}^{N_l} 2h^{(k)}\right) + E_{xx}^{(2)}2h^{(2)}\left(z_2 + \sum_{k=3}^{N_l} 2h^{(k)}\right) + E_{xx}^{(3)}2h^{(3)}\left(z_3 + \sum_{k=4}^{N_l} 2h^{(k)}\right) + \dots\right] + E_{xx}^{(1)}z_0$$

$$= \frac{1}{2h}\sum_{k=1}^{N_l} E_{xx}^{(k)}2h^{(k)}\frac{2h}{2} + E_{xx}^{(1)}z_0 \qquad (\mathrm{A.9})$$

and because $b\sum_{k=1}^{N_l} E_{xx}^{(k)}2h^{(k)} = A_{11}$ we simplify to

$$\therefore \frac{B_{11}}{A} + \frac{1}{2h}\int_{z_0}^{z_{N_l}} \tau_u^{(k)}\mathrm{d}z = \frac{A_{11}}{2b} + E_{xx}^{(1)}z_0. \qquad (\mathrm{A.10})$$

For the second term in Eq. (A.8) we use the same algebraic sequence of steps with

$$D_{11} = b\sum_{k=1}^{N_l} E_{xx}^{(k)}\left(z_k^2 + z_k z_{k-1} + z_{k-1}^2\right)\frac{2h^{(k)}}{3}$$

$$\frac{1}{2h}\int_{z_0}^{z_{N_l}} \tau_\theta^{(k)}\mathrm{d}z = \frac{1}{2h}\sum_{k=1}^{N_l}\left\{E_{xx}^{(k)}\left(z_k^2 + z_k z_{k-1} + z_{k-1}^2\right)\frac{2h^{(k)}}{6} + b^{(k)}2h^{(k)}\right\}$$

and make the final substitution $b \sum\limits_{k=1}^{N_l} E_{xx}^{(k)} (z_k + z_{k-1}) \dfrac{2h^{(k)}}{2} = B_{11}$ to obtain the expression

$$\therefore \frac{D_{11}}{A} + \frac{1}{2h} \int_{z_0}^{z_{N_l}} \tau_\theta^{(k)} \mathrm{d}z = \frac{B_{11}}{2b} + E_{xx}^{(1)} \frac{z_0^2}{2}. \tag{A.11}$$

For the third term in Eq. (A.8) we again use the same algebraic sequence of steps with

$$D_{12} = b \sum_{k=1}^{N_l} E_{xx}^{(k)} \left\{ \beta^{(k)} \left(z_k^2 + z_k z_{k-1} + z_{k-1}^2 \right) \frac{2h^{(k)}}{3} + \alpha^{(k)} (z_k + z_{k-1}) \frac{2h^{(k)}}{2} \right\}$$

$$\frac{1}{2h} \int_{z_0}^{z_{N_l}} \tau_\psi^{(k)} \mathrm{d}z = \frac{1}{2h} \sum_{k=1}^{N_l} E_{xx}^{(k)} \left\{ \beta^{(k)} \left(z_k^2 + z_k z_{k-1} + z_{k-1}^2 \right) \frac{2h^{(k)}}{6} + \alpha^{(k)} (z_k + z_{k-1}) \frac{2h^{(k)}}{2} + c^{(k)} 2h^{(k)} \right\}$$

and finally using $b \sum\limits_{k=1}^{N_l} E_{xx}^{(k)} \left[\beta^{(k)} (z_k + z_{k-1}) \dfrac{2h^{(k)}}{2} + \alpha^{(k)} 2h^{(k)} \right] = B_{12}$ we arrive at

$$\therefore \frac{D_{12}}{A} + \frac{1}{2h} \int_{z_0}^{z_{N_l}} \tau_\psi^{(k)} \mathrm{d}z = \frac{B_{12}}{2b} + E_{xx}^{(1)} \left(\beta^{(1)} \frac{z_0^2}{2} + \alpha^{(1)} z_0 \right) \tag{A.12}$$

Now using Eqs. (A.3), (A.5), (A.7), (A.10), (A.11) and (A.12) at the bottom of the laminate we obtain

$$T_0^{(1)}(z_0) = \frac{\hat{T}_s}{2b} - \frac{\hat{T}_d}{A_{11}} \left[\frac{A_{11}}{2b} + E_{xx}^{(1)} z_0 - E_{xx}^{(1)} z_0 \right] = \frac{b \left(\hat{T}_t + \hat{T}_b \right)}{2b} - \frac{b \left(\hat{T}_t - \hat{T}_b \right)}{2b} = \hat{T}_b \tag{A.13}$$

$$T_\theta^{(1)}(z_0) = -\frac{B_{11}}{A_{11}} \left[\frac{A_{11}}{2b} + E_{xx}^{(1)} z_0 - E_{xx}^{(1)} z_0 \right] + \frac{B_{11}}{2b} + E_{xx}^{(1)} \frac{z_0^2}{2} - E_{xx}^{(1)} \frac{z_0^2}{2} = -\frac{B_{11}}{2b} + \frac{B_{11}}{2b} = 0 \tag{A.14}$$

$$T_\psi^{(1)}(z_0) = -\frac{B_{12}}{A_{11}} \left[\frac{A_{11}}{2b} + E_{xx}^{(1)} z_0 - E_{xx}^{(1)} z_0 \right] + \frac{B_{12}}{2b} + E_{xx}^{(1)} \left(\beta^{(1)} \frac{z_0^2}{2} + \alpha^{(1)} z_0 \right) - E_{xx}^{(1)} \left(\beta^{(1)} \frac{z_0^2}{2} + \alpha^{(1)} z_0 \right)$$

$$= -\frac{B_{12}}{2b} + \frac{B_{12}}{2b} = 0 \tag{A.15}$$

Similarly using Eqs. (A.2), (A.4), (A.6), (A.10), (A.11) and (A.12) at the top of the laminate we obtain

$$T_0^{(N_l)}(z_{N_l}) = \frac{\hat{T}_s}{2b} - \frac{\hat{T}_d}{A_{11}} \left[\frac{A_{11}}{2b} + E_{xx}^{(1)} z_0 - \frac{A_{11}}{b} - E_{xx}^{(1)} z_0 \right] = \frac{b \left(\hat{T}_t + \hat{T}_b \right)}{2b} + \frac{b \left(\hat{T}_t - \hat{T}_b \right)}{2b} = \hat{T}_t \tag{A.16}$$

$$T_\theta^{(N_l)}(z_{N_l}) = -\frac{B_{11}}{A_{11}} \left[\frac{A_{11}}{2b} + E_{xx}^{(1)} z_0 - \frac{A_{11}}{b} - E_{xx}^{(1)} z_0 \right] + \frac{B_{11}}{2b} + E_{xx}^{(1)} \frac{z_0^2}{2} - \frac{B_{11}}{b} - E_{xx}^{(1)} \frac{z_0^2}{2} = \frac{B_{11}}{2b} - \frac{B_{11}}{2b} = 0 \tag{A.17}$$

$$T_\psi^{(N_l)}(z_{N_l}) = -\frac{B_{12}}{A_{11}} \left[\frac{A_{11}}{2b} + E_{xx}^{(1)} z_0 - \frac{A_{11}}{b} - E_{xx}^{(1)} z_0 \right] + \frac{B_{12}}{2b} + E_{xx}^{(1)} \left(\beta^{(1)} \frac{z_0^2}{2} + \alpha^{(1)} z_0 \right)$$

$$-\frac{B_{12}}{b} - E_{xx}^{(1)} \left(\beta^{(1)} \frac{z_0^2}{2} + \alpha^{(1)} z_0 \right) = \frac{B_{12}}{2b} - \frac{B_{12}}{2b} = 0 \qquad \text{(A.18)}$$

Therefore, by substituting the expressions of Eq. (A.13)-(A.18) into Eq. (A.1) we have

$$\tau_{xz(a)}^{(1)} (z_0) = \hat{T}_b + 0 \times f_\theta + 0 \times f_\psi = \underline{\underline{\hat{T}_b}}$$

$$\tau_{xz(a)}^{(N_l)} (z_{N_l}) = \hat{T}_t + 0 \times f_\theta + 0 \times f_\psi = \underline{\underline{\hat{T}_t}}$$

and therefore the transverse shear stresses at the top and bottom of the laminate are exactly recovered.

Appendix B. Constrained anisoparametric shape functions

In RZT$^{(m)}$ the transverse shear force is given by Eq. (37). Hence,

$$V = Q_{11}^m (w_{,x} + \theta) + Q_{12}^m \psi + Q_{10}^m = Q_{11}^m \{(w_{,x} + \theta) + r\psi\} + Q_{10}^m \qquad \text{(B.1)}$$

where $r = Q_{12}^m / Q_{11}^m$. Using the anisoparametric shape functions in Eq. (50) we can write:

$$(w_{,x} + \theta) + r\psi = \frac{2}{L^{(e)}} \left(\xi - \frac{1}{2} \right) w_1 - \frac{4}{L^{(e)}} \xi w_3 + \frac{2}{L^{(e)}} \left(\xi + \frac{1}{2} \right) w_2 + \frac{1}{2} (1 - \xi) \theta_1 + \frac{1}{2} (1 + \xi) \theta_2 +$$
$$\frac{r}{2} (1 - \xi) \psi_1 + \frac{r}{2} (1 + \xi) \psi_2$$

$$(w_{,x} + \theta) + r\psi = \xi \left\{ \frac{2}{L^{(e)}} w_1 - \frac{4}{L^{(e)}} w_3 + \frac{2}{L^{(e)}} w_2 + \frac{1}{2} (\theta_2 - \theta_1) + \frac{r}{2} (\psi_2 - \psi_1) \right\} +$$
$$\left(\frac{w_2 - w_1}{L^{(e)}} + \frac{\theta_1 + \theta_2}{2} + r \frac{\psi_1 + \psi_2}{2} \right). \qquad \text{(B.2)}$$

Now if we choose to constrain the shear force component associated with the kinematics, i.e. $Q_{11}^m \{(w_{,x} + \theta) + r\psi\}$ in Eq. (B.1), to be constant, then the coefficient of the ξ term in Eq. (B.2) must vanish. Hence, using this condition we can find an expression for the mid-element nodal deflection w_3:

$$\frac{2}{L^{(e)}} w_1 - \frac{4}{L^{(e)}} w_3 + \frac{2}{L^{(e)}} w_2 + \frac{1}{2} (\theta_2 - \theta_1) + \frac{r}{2} (\psi_2 - \psi_1) = 0$$
$$\therefore w_3 = \frac{w_1 + w_2}{2} + \frac{L^{(e)}}{8} \{\theta_2 - \theta_1 + r (\psi_2 - \psi_1)\} \qquad \text{(B.3)}$$

As a result, the w_3 degree of freedom in the standard quadratic Lagrange shape functions of

Eq. (50), i.e.

$$w = H_1^Q w_1 + H_3^Q w_3 + H_2^Q w_2, \tag{B.4}$$

can be replaced to give

$$w = H_1^L w_1 + H_2^L w_2 + \frac{L^{(e)}}{8} \left(1 - \xi^2\right) \left\{\theta_2 - \theta_1 + r\left(\psi_2 - \psi_1\right)\right\}. \tag{B.5}$$

Finally, if we constrain $\eta = w_{,x} + \theta - \psi$ to be constant, then the term $r\psi$ in Eq. (B.5) becomes $-\psi$ and hence

$$w_3 = \frac{w_1 + w_2}{2} + \frac{L^{(e)}}{8} \left\{\theta_2 - \theta_1 - \left(\psi_2 - \psi_1\right)\right\} \tag{B.6}$$

and subsequently

$$w = H_1^L w_1 + H_2^L w_2 + \frac{L^{(e)}}{8} \left(1 - \xi^2\right) \left\{\theta_2 - \theta_1 - \left(\psi_2 - \psi_1\right)\right\}. \tag{B.7}$$

References

[1] L Demasi. Partially zig-zag advanced higher order shear deformation theories based on the generalized unified formulation. *Composite Structures*, 94(2):363–375, 2012.

[2] G Kirchhoff. Uber das Gleichgewicht und die Bewegung einer elastischen Scheibe. *Journal fur reine und angewandte Mathematik*, 40:51–88, 1850.

[3] AEH Love. *The Mathematical Theory of Elasticity*. Cambridge University Press, London, 1934.

[4] RM Jones. *Mechanics of Composite Materials*. Taylor & Francis Ltd, London, UK, 2nd edition, 1998.

[5] RD Mindlin. Influence of rotary inertia and shear on flexural motion of isotropic elastic plates. *Journal of Applied Mechanics*, 18:31–38, 1951.

[6] PC Yang, CH Norris, and Y Stavsky. Elastic wave propagation in heterogeneous plates. *International Journal of Solids and Structures*, 2:665–684, 1966.

[7] M Levinson. A new rectangular beam theory. *Journal of Sound and Vibration*, 74(1):81–87, 1981.

[8] JN Reddy. A refined nonlinear theory of plates with transverse shear deformation. *International Journal of Solids and Structures*, 20(9):881–896, 1983.

[9] FB Hildebrand, E Reissner, and GB Thomas. Notes on the foundations of the theory of small displacements of orthotropic shells. Technical Note 1833, National Advisory Committee for Aeronautics, 1938.

[10] KH Lo, RM Christensen, and EM Wu. A high-order theory of plate deformation - Part 2: Laminated plates. *Journal of Applied Mechanics*, 44(4):669–676, 1977.

[11] SG Lekhnitskii. Strength calculation of composite beams. *Vestn. Inzh. Tekh*, 9, 1935.

[12] SA Ambartsumyan. On a general theory of anisotropic shells. *Prikl. Mat. Mekh*, 22:226–237, 1958.

[13] M Di Sciuva. A refinement of the transverse shear deformation theory for multilayered orthotropic plates. *L'aerotecnica missile e spazio*, 62:84–92, 1984.

[14] H Murakami. Laminated composite plate theory with improved in-plane responses. *Journal of Applied Mechanics*, 53:661–666, 1986.

[15] A Tessler, M Di Sciuva, and M Gherlone. Refinement of Timoshenko beam theory for composite and sandwich beams using zigzag kinematics. Technical Publication 215086, National Aeronautics and Space Administration, 2007.

[16] A Tessler, M Di Sciuva, and M Gherlone. Refined zigzag theory for laminated composite and sandwich plates. Technical Publication 215561, National Aeronautics and Space Administration, 2009.

[17] A Tessler, M Di Sciuva, and M Gherlone. Refined zigzag theory for homogeneous, laminated composite, and sandwich plates: A homogeneous limit methodology for zigzag function selection. Technical Publication 216214, National Aeronautics and Space Administration, 2010.

[18] A Tessler, M Di Sciuva, and M Gherlone. A consistent refinement of first-order shear deformation theory for laminated composite and sandwich plates using improved zigzag kinematics. *Journal of Mechanics of Materials and Structures*, 5(2):341–367, 2010.

[19] U Icardi and F Sola. Assessment of recent zig-zag theories for laminated and sandwich structures. *Composites Part B*, 97:26–52, 2016.

[20] E Carrera. Developments, ideas and evaluations based upon Reissner's mixed variational theorem in the modeling of multilayered plates and shells. *Applied Mechanics Reviews*, 54(4):301–329, 2001.

[21] JM Whitney. Stress analysis of thick laminated composite and sandwich plates. *Journal of Composite Materials*, 6(4):426–440, 1972.

[22] A Tessler and HR Riggs. Accurate interlaminar stress recovery from Finite Element Analysis. Technical Memorandum 109149, NASA, 1994.

[23] R Rolfes and K Rohwer. Improved transverse shear stresses in composite finite elements based on first order shear deformation theory. *International Journal for Numerical Methods in Engineering*, 40:51–60, 1997.

[24] R Rolfes, K Rohwer, and M Ballerstaedt. Efficient linear transverse normal stress analysis of layered composite plates. *Computers & Structures*, 68(6):643–652, 1998.

[25] G Kuhlmann and R Rolfes. A hierarchic 3D finite element for laminated composites. *International Journal for Numerical Methods in Engineering*, 61:96–116, 2004.

[26] E Reissner. On the theory of bending of elastic plates. *Journal of Mathematics and Physics*, 23:184–191, 1944.

[27] E Reissner. The effect of transverse shear deformation on the bending of elastic plates. *Journal of Applied Mechanics*, 12(30):A69–A77, 1945.

[28] RC Batra and S Vidoli. Higher-order piezoelectric plate theory derived from a three-dimensional variational principle. *AIAA Journal*, 40(1):91–104, 2002.

[29] RMJ Groh and PM Weaver. A computationally efficient 2D model for inherently equilibrated 3D stress predictions in heterogeneous laminated plates. Part II: Model validation. *Composite Structures*, 2015.

[30] E Reissner. On a certain mixed variational theorem and a proposed application. *International Journal for Numerical Methods in Engineering*, 20(7):1366–1368, 1984.

[31] RMJ Groh and PM Weaver. On displacement-based and mixed-variational equivalent single layer theories for modelling highly heterogeneous laminated beams. *International Journal of Solids and Structures*, 59:147–170, 2015.

[32] M Gherlone. On the use of zigzag functions in equivalent single layer theories for laminated composite and sandwich beams: A comparative study and some observations on external weak layers. *Journal of Applied Mechanics*, 80:1–19, 2013.

[33] A Tessler. Refined zigzag theory for homogeneous, laminated composite, and sandwich beams derived from Reissner's mixed variational principle. *Meccanica*, Advances In The Mechanics Of Composite And Sandwich Structures:1–26, 2015.

[34] L Iurlaro, M Gherlone, M Di Sciuva, and A Tessler. Refined zigzag theory for laminated composite and sandwich plates derived from Reissner's mixed-variational theorem. *Composite Structures*, 133:809–817, 2015.

[35] M Gherlone, A Tessler, and M Di Sciuva. C0 beam elements based on the refined zigzag theory for multilayered composite and sandwich laminates. *Composite Structures*, 93:2882–2894, 2011.

[36] A Tessler and S Dong. On a hierarchy of conforming Timoshenko beam elements. *Computers & Structures*, 14(3–4):335–344, 1981.

[37] M Di Sciuva, M Gherlone, L Iurlaro, and A Tessler. A class of higher-order C0 composite and sandwich beam elements based on the refined zigzag theory. *Composite Structures*, 132:784–803, 2015.

[38] L Iurlaro, M Gherlone, and M Di Sciuva. The (3,2)-mixed Refined Zigzag Theory for generally laminated beams: Theoretical development and C0 finite element formulation. *International Journal of Solids and Structures*, 73-74:1–19, 2015.

[39] A Eijo, E Oate, and S Oller. A numerical model of delamination in composite laminated beams using the LRZ beam element based on the refined zigzag theory. *Composite Structures*, 104:270–280, 2013.

[40] RMJ Groh, PM Weaver, and A Tessler. Application of the Refined Zigzag Theory to the modeling of delaminations in laminated composites. Technical Memorandum NASA/TM-2015-218808, NASA, 2015.

[41] RMJ Groh and PM Weaver. A computationally efficient 2D model for inherently equilibrated 3D stress predictions in heterogeneous laminated plates. Part I: Model formulation. *Composite Structures*, 2015.

[42] C Thurnherr, RMJ Groh, P Ermanni, and PM Weaver. Higher-order beam model for stress predictions in curved beams made from anisotropic materials. *International Journal of Solids and Structures*, 2016.

[43] NJ Pagano. Exact solutions for composite laminates in cylindrical bending. *Journal of Composite Materials*, 3(3):398–411, 1969.

[44] GC Everstine and AC Pipkin. Stress channelling in transversely isotropic elastic composites. *Zeitung fuer angewandte Mathematik und Physik*, 22(5):825–834, 1971.